Using the chemical equilibrium partitioning space to explore factors influencing the phase distribution of compounds involved in secondary organic aerosol formation

F. Wania,[1,2,*] Y. D. Lei,[1,2,3] C. Wang,[1,2] J. P. D. Abbatt,[2] K.-U. Goss[4,5]

[1]{Department of Physical and Environmental Sciences, University of Toronto Scarborough, 1265 Military Trail, Toronto, Ontario, Canada M1C 1A4}

[2]{Department of Chemistry, University of Toronto, Toronto, Ontario, M1C 1A4, Canada}

[3]{Department of Chemical Engineering and Applied Chemistry, University of Toronto, Toronto, Ontario, M1C 1A4, Canada}

[4]{Department of Analytical Environmental Chemistry, Centre for Environmental Research UFZ Leipzig-Halle, Permoserstraße 15, D-04318 Leipzig, Germany}

[5]{Institute of Chemistry, University of Halle-Wittenberg, Kurt-Mothes-Straße 2, D-06120 Halle, Germany}

Correspondence to: F. Wania (frank.wania@utoronto.ca)

Abstract

Many atmospheric and chemical variables influence the partitioning equilibrium between gas phase and condensed phases of compounds implicated in the formation of secondary organic aerosol (SOA). The large number of factors and their interaction makes it often difficult to assess their relative importance and concerted impact. Here we introduce a two-dimensional space, which maps regions of dominant atmospheric phase distribution within a coordinate system defined by equilibrium partition coefficients between the gas phase, an aqueous phase and a water insoluble organic matter (WIOM) phase. Placing compounds formed from the oxidation of *n*-alkanes, terpenes and mono-aromatic hydrocarbons on the maps based on their predicted partitioning properties allows for a simple graphical assessment of their equilibrium phase distribution behaviour. Specifically, it allows for the simultaneous visualization and quantitative comparison of the impact on phase distribution of changes in atmospheric parameters (such as temperature, salinity, WIOM phase polarity, organic aerosol load, and liquid water content), and chemical properties (such as oxidation state, molecular size, functionalization, and dimerisation). The graphical analysis reveals that the addition of hydroxyl, carbonyl and carboxyl groups increases the affinity of aliphatic, alicyclic and aromatic hydrocarbons for the aqueous phase more rapidly than their affinity for WIOM, suggesting that the aqueous phase may often be relevant even for substances that are considerably larger than the C2 and C3 compounds that are typically believed to be associated with aqueous SOA. In particular, the maps identify some compounds that contribute to SOA formation if partitioning to both WIOM and aqueous phase is considered, but would remain in the gas phase if either condensed phase were neglected. For example, many semi-volatile α-pinene oxidation products will contribute to aqueous SOA under the high liquid water content conditions encountered in clouds, but would remain vapours in wet aerosol. It is conceivable to develop parameterizations of "partitioning basis sets" that group compounds with comparable partitioning properties, which - when combined with data on the abundance of those groups of compounds – could serve in the simulation of SOA formation.

1 Introduction

The phase distribution of oxidized organic compounds between the gas phase and the condensed phases present in the atmosphere, and how that distribution is affected by atmospheric and chemical variables, is central to the understanding and quantification of the formation of secondary organic aerosol (SOA) (Hallquist et al., 2009). For example, the molecular size of the compounds and the functional groups they contain have a strong influence on their preference for either gas phase or the condensed phase(s) making up an aerosol particle. Atmospheric temperature strongly impacts that phase equilibrium. The concentration and the polarity of the organic particulate matter present in the atmosphere play a role, as do relative humidity and the resultant liquid water content of the atmosphere. The presence of electrolytes such as ammonium sulphate and sodium chloride further modifies the gas phase-aqueous phase equilibrium. How all these variables impact gas/particle partitioning is reasonably well understood and in most cases can even be quantified with some confidence (e.g. Zuend and Seinfeld, 2012, Shiraiwa et al., 2013). Nevertheless, due to the large number of the variables and their interaction, it is often difficult to assess the relative importance of each of these variables and to fully comprehend the concerted impact of all of them acting together. In fact, different variables will be important for different chemicals and under different atmospheric circumstances.

Graphical methods illustrating the effect of multiple variables within a common framework can be a powerful tool for understanding their relative importance and concerted impact (e.g. Wong and Wania, 2011). They can also aid in the identification and prioritization of data gaps by indicating for which compounds and which circumstances a more precise quantification of the effect of a variable on phase partitioning is required and when approximate knowledge can be tolerated.

Ten years ago, we introduced the chemical partitioning space as a graphical method for furthering the understanding of the concerted impact of multiple variables on the phase distribution of semi-volatile organic trace contaminants, such as polycyclic aromatic hydrocarbons and polychlorinated biphenyls, in the atmosphere (Lei and Wania, 2004). The basic idea of the chemical partitioning space is to calculate and display regions of dominant phase distribution within a coordinate system defined by equilibrium phase partition coefficients, and then to place substances on the resulting maps based on their partitioning properties under certain prevailing conditions (e.g. of temperature). This allows for a simple graphical assessment

of the substances' equilibrium phase distribution behaviour and in turn of their depositional and reactive fate (Lei and Wania, 2004, Westgate and Wania, 2013). We believe, and seek to demonstrate here, that the chemical partitioning space could also be used to gain a deeper appreciation of the impact of various chemical and atmospheric variables on the phase distribution behaviour of SOA compounds. Because SOA formation strongly depends on the phase distribution behaviour of those substances, this also amounts to an exploration of the impact of those variables on the likelihood and the extent of SOA formation, as well as on the nature of the SOA formed.

The atmospheric chemistry community has a long tradition of using graphical tools to illustrate and advance understanding of atmospheric processes (e.g. Pankow and Barsanti 2009, Heald et al., 2010, Kroll et al., 2011, Isaacman et al., 2011, Donahue et al. 2011, 2012, Cappa and Wilson, 2012) and there are precedents of displaying the phase distribution behaviour of SOA compounds as a function of chemical equilibrium partitioning parameters. The Volatility Basis Set (VBS) approach by Donahue and co-workers (2006, 2011, 2012) in both its one-dimensional and two-dimensional manifestations, is sometimes used to indicate the distribution between gas and particle phase as a function of organic aerosol load and a compound's saturation concentration, which is defined as the reciprocal of a gas-particle partition coefficient and typically derived from saturation vapour pressure (Donahue et al., 2006). Similarly, Volkamer et al. (2009) displayed the distribution of glyoxal between gas and aqueous phase as a function of an effective Henry's law constant and the atmospheric liquid water content. However, to the best of our knowledge, no attempt has been made so far to similarly display graphically the distribution behaviour of SOA compounds between the gas phase, the atmospheric liquid water phase, and the organic aerosol phase at the same time. Notably, the two-dimensional representations of organic compounds used in the SOA community employ a chemical equilibrium partitioning parameter for at most one of the two dimensions and thus do not have a sole focus on phase distribution. Even if they do consider phase distribution behaviour (e.g. the 2D VBS, Donahue et al., 2011, 2012), the existence of a liquid water phase in the atmosphere is ignored. Recently, Hodzic et al. (2014) placed SOA compounds in a two-dimensional space defined by saturation concentration and effective Henry's law constant in order to observe and derive relationships between these two parameters for different groups of SOA compounds.

After first introducing the chemical partitioning space for the atmosphere, we explain how to place SOA compounds within the space and how to account for the influence of various variables on that placement. Using the partitioning space we then illustrate the impact of prediction uncertainty, temperature, salting-out effect, phase polarity, liquid water content, organic aerosol load, and chemical ageing (i.e. functionalization and oligomerisation) on the phase distribution of selected oxidation products of *n*-alkanes, biogenic terpenes and aromatic hydrocarbons.

2 Methods

2.1 Defining the Chemical Partitioning Space

The equilibrium partition coefficient of a chemical between two phases X and Y is defined as:

$$K_{X/Y} = \frac{C_X}{C_Y} \qquad \text{eq. 1}$$

where C_X and C_Y are the concentrations in phase X and Y in units of mol per m^3 of phase. $K_{X/Y}$ thus has units of m^3 of phase Y per m^3 of phase X. In a system consisting of the gas phase (G), an aqueous phase (W) and a water insoluble organic matter phase (WIOM) there are three partition coefficients, which are related to each other according to:

$$K_{W/G} = \frac{K_{W/WIOM}}{K_{G/WIOM}} \qquad \text{eq. 2}$$

Two of the three coefficients are therefore sufficient to describe a chemical's relative preferences for the three phases. Two coefficients in logarithmic form can be used to define a two dimensional coordinate system, which we call the chemical partitioning space. In Fig. 1A, log $K_{W/G}$ and log $K_{WIOM/G}$ are used to define such a space.

The equilibrium partition coefficient between WIOM and the gas phase ($K_{WIOM/G}$) on the x-axis is related to the gas-particle partition coefficient K' in units of $m^3/\mu g$ (Pankow, 2003) through:

$$K_{WIOM/G} = K' \delta_{WIOM} \frac{10^6 \mu g}{g} \qquad \text{eq. 3}$$

where δ_{WIOM} is the density of WIOM in units of g/m^3. The equilibrium partition coefficient between water and gas phase $K_{W/G}$ on the y-axis is related to the Henry's Law constants H in

130 units of mol Pa^{-1} m^{-3}, or to *H'* in the non-SI units of M/atm favoured by the atmospheric
131 chemistry community, through:

132 $$K_{W/G} = HRT = H'RT \times \frac{1\ atm\ L}{101.325\ Pa\ m^3} \quad \text{eq. 4}$$

133 where *R* is the ideal gas constant (8.314 Pa m^3 K^{-1} mol^{-1}) and *T* is absolute temperature in K. A
134 chemical can be placed in such a coordinate system based on its equilibrium partition
135 coefficients.

136 We should mention that the use of term WIOM does not imply that the compounds making up
137 this phase necessarily have low water solubility. Even relatively water-soluble compounds can
138 have a higher preference for solvation in an organic phase than in a mostly aqueous phase.

139 2.2 Displaying Chemical Phase Distribution in the Partitioning Space

140 If a three-phase system consisting of gas, water and WIOM is at chemical equilibrium, the
141 fraction Φ_X of the total amount of a chemical that is in one of the three phases can be calculated
142 using (Lei and Wania, 2004):

143 $$\phi_G = 1/(1 + K_{W/G}\frac{V_W}{V_G} + K_{WIOM/G}\frac{V_{WIOM}}{V_G}) \quad \text{eq. 5}$$

144 $$\phi_W = 1/(1 + K_{G/W}\frac{V_G}{V_W} + K_{WIOM/W}\frac{V_{WIOM}}{V_W}) \quad \text{eq. 6}$$

145 $$\phi_{WIOM} = 1/(1 + K_{G/WIOM}\frac{V_G}{V_{WIOM}} + K_{W/WIOM}\frac{V_W}{V_{WIOM}}) \quad \text{eq. 7}$$

146 This means that the chemical's phase distribution depends only on its equilibrium partition
147 coefficients and the phase volumes V_X in m^3. In the atmosphere V_W and V_{WIOM} are negligibly
148 small compared to V_G and the volume ratios V_W/V_G and V_{WIOM}/V_G can be calculated from the
149 liquid water content (LWC) and the organic aerosol load (OAL) in units of μg/m^3 using:

150 $$\frac{V_W}{V_G} = LWC\ in\ \mu g/m^3 \times 10^{-6}\frac{g}{\mu g} \times 10^{-6}\frac{m^3}{g} \quad \text{eq. 8}$$

151 $$\frac{V_{WIOM}}{V_G} = OAL\ in\ \mu g/m^3 \times 10^{-6}\frac{g}{\mu g} \times 10^{-6}\frac{m^3}{g} \quad \text{eq. 9}$$

152 We thereby assume that water and WIOM have a density of 10^6 g/m^3.

If we now assume LWC and OAL to be fixed, the phase distribution as calculated in equations 5 to 7 only depends on the partition coefficients and we can display the values of Φ_G, Φ_W, and Φ_{WIOM} within the partitioning space. In Fig. 1A this has been done assuming a LWC of 10 μg/m^3 and an OAL of 10 μg/m^3. In the red-coloured, upper left of the partitioning space are chemicals with low $K_{W/G}$ and low $K_{WIOM/G}$, i.e. chemical favouring the gas phase over the aqueous phase and WIOM. Accordingly they are predominately in the gas phase (different shades of red are used to indicate areas of the space where Φ_G exceeds 50%, 90% and 99%). In the blue-coloured lower left of the space are chemicals with high $K_{W/G}$ and low $K_{WIOM/G}$, i.e. highly water-soluble chemicals that favour the gas phase over the WIOM phase and thus partition predominantly into the aqueous phase (different shades of blue indicate areas of the space where Φ_W exceeds 50%, 90% and 99%). Finally, in the green-coloured upper right of the space are chemicals with low $K_{W/G}$ and high $K_{WIOM/G}$, i.e. sparingly water-soluble substances of low volatility, that partition predominantly into the WIOM phase (different shades of green indicate areas of the space where Φ_{WIOM} exceeds 50%, 90% and 99%).

The lines between the fields coloured in red, blue and green ($\Phi_G = \Phi_W = \Phi_{WIOM} = 50\%$) indicate the $K_{W/G}$ and $K_{WIOM/G}$ thresholds, where the transition of chemicals from mostly in the gas phase to mostly in the aqueous or WIOM phase occurs (Fig. 1A). The vertical threshold between predominant partitioning into gas and WIOM phase occurs at $\log K_{WIOM/G} = \log (V_G/V_{WIOM})$ and the horizontal threshold between predominant partitioning into gas and aqueous phase at $\log K_{W/G} = \log (V_G/V_W)$. At the assumed LWC and OAL of 10 μg/m^3 this corresponds to $\log K_{W/G}$ and $\log K_{WIOM/G}$ values of 11.

Because of the thermodynamic relationship of eq. 2, $K_{WIOM/W}$ equals $K_{WIOM/G}$ divided by $K_{W/G}$ and diagonal lines from the upper left to the lower right in the partitioning space designate lines of equal $K_{WIOM/W}$. The diagonal lines in the lower right of Figure 1A therefore show where the transition from dominant partitioning into WIOM and aqueous phase takes place. If liquid water and WIOM are equally abundant (LWC and OAL is 10 μg/m^3) the threshold falls at $\log K_{WIOM/G} = \log (V_G/V_{WIOM}) = \log 1 = 0$. This threshold could obviously also be calculated from the other two thresholds ($\log K_{WIOM/G} - \log K_{W/G} = 11 - 11 = 0 = \log K_{WIOM/G}$). The white triangle in the centre of the three coloured areas designates the partitioning properties of chemicals that partition to none of the three phases to more than 50 %, i.e. they are present in equal proportions in all three phases. Finally, the two triangular areas with bow-shaped flanks, surrounding the

white triangle and being delineated by dashed lines, encompass properties of chemicals that partition mostly in one phase, with the remainder split between the other two phases.

Of course, the thresholds are not fixed, but depend on the size of the aqueous and WIOM phase in the atmosphere. OAL in the atmosphere ranges between 0.1 and 100 $\mu g/m^3$, with most measurements yielding OAL between 1 and 10 $\mu g/m^3$ (Jimenez et al., 2009). In Fig. 1B, broken vertical lines indicate where the threshold between predominant partitioning into gas and WIOM phase would fall, if OALs of 0.1, 1, and 100 $\mu g/m^3$ prevailed. With each order of magnitude increase in the OAL, the threshold moves one log unit to the left, i.e. more volatile chemicals (i.e. with lower log $K_{WIOM/G}$) will shift their equilibrium phase distribution from the gas to the WIOM phase. Similarly, the broken horizontal lines in Fig. 1B indicate the threshold between predominant partitioning into gas and aqueous phase, if larger or lower volumes of water were associated with the aerosol, i.e. at LWCs of 100 or 1 $\mu g/m^3$, respectively. With each order of magnitude increase in the LWC, the threshold moves one log unit up, i.e. more volatile chemicals (i.e. with lower log $K_{W/G}$) will shift their phase distribution from the gas to the aqueous phase.

The amount of liquid water in an aerosol depends on temperature, relative humidity and on the particle concentration and type, i.e. its hygroscopicity. A range of LWC between 1 and 100 $\mu g/m^3$ was deemed plausible based on calculations with the E-AIM model (Wexler and Clegg, 2002). At high relative humidity and if the aerosol particles can act as cloud condensation nuclei, water starts to condense to a much greater extent and the LWC will adopt values that are more than 5 orders of magnitude higher. Fig. 1C thus maps Φ_G, Φ_W, and Φ_{WIOM} for a LWC of 0.3 g/m3 (V_W/V_G= $3x10^{-7}$ m^3/m^3)), which is typical for conditions within a cloud. The horizontal threshold moves sharply higher to a log $K_{W/G}$ of 6.5, which means that at equilibrium many more chemicals will partition into the aqueous phase of a cloud, than in an aerosol under clear sky conditions (Fig. 1B). We note that the left side of the partitioning space plots is similar to a figure illustrating the partitioning of water-soluble molecules to cloud, fog and aerosol liquid water presented previously (Fig. 8 in Volkamer et al., 2009).

In atmospheric chamber experiments conducted at low relative humidity, the liquid water content of aerosol may be negligibly low. In that case the fraction in the aqueous phase Φ_W is also negligible, and the blue field disappears from the partitioning space altogether (Fig. 1D), or

rather the vertical threshold moves so far down to no longer fall within the range of displayed $K_{W/G}$ values. During some chamber experiments, OAL exceed levels observed in ambient air, (e.g. 1000 μg/m^3) and the vertical threshold can move far to the left, i.e. to a log $K_{WIOM/G}$ of around 9 (Fig. 1D).

We should stress that while Figures 1B to 1D only show the threshold for shifts in dominant phase partitioning, i.e. the lines where 50 % of a chemical is in one phase, even very small fractions of a chemical partitioning into a phase could be important, for example, if they have an efficient reactive or depositional sink within that phase or if they have reached high concentrations in their preferred phases.

2.3 Major Assumptions Underlying the Chemical Partitioning Space Approach

Before proceeding to consider and interpret chemical partitioning space plots for SOA compounds, it is worthwhile to discuss two major assumptions that are made when drawing these diagrams. The first assumption is that chemicals achieve quasi-instantaneous equilibrium between the phases present in the atmosphere. The second is that the condensed phase separates into a largely aqueous phase and a phase largely made up of water-insoluble organic matter. In particular, we do not consider the possibility of the simultaneous presence of two immiscible, largely non-aqueous organic phases, e.g. a non-polar hydrocarbon-like phase separated from a polar, highly oxidized, non-aqueous phase. (Such a phase separation is for example predicted by the 2D VBS approach (Donahue et al., 2012), but this approach also disregards the presence of water in the condensed phase.) Because of the equilibrium assumption, particle morphology, i.e. the spatial arrangement of the two condensed phases relative to each other, is of no concern in our analysis (Shiraiwa et al., 2013).

While for a long time, the time scale of chemical diffusion in largely liquid-like atmospheric aerosol phases was judged sufficiently short to assume that equilibrium partitioning prevails most of the time, more recently evidence is emerging that suggests that the physical state of organic aerosol may at times be semi-solid or glassy (Mikhailov et al., 2009, Virtanen et al., 2010) and the rate of mass transfer in such phases is too slow to assure equilibrium distribution at atmospheric time scales (e.g. Koop et al., 2011, Perraud et al., 2012). However, this view is not yet universally acknowledged and there is similarly experimental evidence of the validity of

243 the quasi-instantaneous equilibrium assumption (e.g. Saleh et al., 2013). In any case, even if
244 chemical equilibrium is not always achieved the equilibrium distribution is still of paramount
245 importance as the state that the system strives to reach.

246 Support for separation into predominantly organic and aqueous phases in aerosol stems from
247 laboratory (e.g. Song et al., 2012), field (You et al., 2012) and theoretical investigations (e.g.
248 Bertram et al., 2011, Zuend and Seinfeld, 2012). These same investigations also suggest the
249 possibility of the formation of a single condensed phase at high relative humidity and if the
250 organic material is highly oxidized. Incidentally, even though we assume the presence of a
251 WIOM phase separate from an aqueous phase when drawing the partitioning space map, the map
252 still can indicate when such phase separation is unlikely. Namely, if most of the organic
253 compounds present in an aerosol fall in the part of the partitioning space indicating predominant
254 partitioning into the aqueous phase and few fall into the part corresponding to partitioning into
255 WIOM, it stands to reason that no WIOM phase will form and that instead all of the organic
256 material present will be in a single condensed phase.

257 ## 2.4 Estimating the Equilibrium Partition Coefficients for SOA Compounds

258 A chemical occupies a place within the chemical partitioning space based on its partition
259 coefficients $K_{W/G}$ and $K_{WIOM/G}$. Ideally, one would use measured partition coefficients to locate a
260 substance in the partitioning space (Lei and Wania, 2004). However, because such data are not
261 available for many, if not most of the substances involved in SOA formation, we need to rely on
262 prediction methods when trying to locate SOA compounds in the chemical partitioning space.
263 We recently applied three such methods to the prediction of $K_{WIOM/G}$ for substances involved in
264 SOA formation (Wania et al., 2014). These methods, which were first applied to the issue of gas-
265 particle partitioning by Arp et al. (2008) and Arp and Goss (2009), are poly-parameter linear free
266 energy relationships (ppLFERs) calibrated with empirical aerosol sorption data, the solvation
267 models implemented in SPARC Performs Automated Reasoning in Chemistry (SPARC) (Hilal et
268 al., 2004), and the quantum-chemical software COSMOtherm (Version C30_1401 with
269 BP_TZVP_C30_1401 parameterization, COSMOlogic GmbH & Co. KG, Leverkusen, Germany,
270 2014), which predict solvation equilibria from molecular structure alone. The same three
271 methods can also be used to predict $K_{W/G}$.

We compiled the chemical identity of compounds believed to form during the oxidation of normal alkanes with 8 to 17 carbons (Jordan et al., 2008), terpenes (Chen and Griffin, 2005) and aromatic hydrocarbons (Forstner et al., 1997). Additional oxidation products of α-pinene were taken from Camredon et al. (2010), Shilling et al. (2009) and Valorso et al. (2011). Molecular structures of a total of more than 350 molecules were drawn with ChemSketch (ACD/Labs, Advanced Chemistry Development Inc. Toronto, Canada), which yields each molecule's SMILES (simplified molecular-input line-entry system) string.

For the ppLFER approach, the molecules' solute descriptors were predicted with ABSOLV, which relies on a group contribution quantitative structure property relationship (ACD/Labs, Toronto, Canada). $K_{W/G}$ at different temperatures were calculated directly using the ppLFER equations given by Goss (2006). $K_{WIOM/G}$ at 15 °C for four different aerosol particles (sampled from urban, suburban, rural and coastal sites during different seasons) were calculated using ppLFER equations by Arp et al. (2008), and adjusted for temperature using an enthalpy of phase partitioning estimated using the approach described in Wania et al. (2014). The temperature-adjusted log $K_{WIOM/G}$ for the four aerosol samples was averaged.

SPARC directly predicts $K_{W/G}$ and $K_{WIOM/G}$ as a function of temperature when provided with a SMILES code. For the $K_{WIOM/G}$ prediction, SPARC requires a solvent to be specified, which should have solvation properties that resemble those of WIOM in SOA (Wania et al., 2014). As a default choice we used a relatively non-polar, hypothetical structure termed B proposed to be an oligomerisation product of the oxidation of volatile aromatics (Kalberer et al., 2004, Arp and Goss, 2009, Wania et al., 2014). For the estimation of $K_{WIOM/G}$ of the oxidation products of α-pinene, we additionally used two molecules as surrogate solvents that are themselves oxidation products of α-pinene: a dimer formed by esterification of pinic acid and 10-hydroxy-pinonic acid, referred to as ESTER_dimer by Zuend and Seinfeld (2012), and 5-hydroperoxy-4-(hydroxymethyl)-5-methyl-2-oxohexanoic acid, designated as C813OOH in the Master Chemical Mechanism model. The latter chemical is highly oxygenated and polar.

Wania et al. (2014) describe the prediction of $K_{WIOM/G}$ for the *n*-alkane oxidation products using COSMOtherm and the surrogate solvent B mentioned above. COSMOtherm was similarly used to calculate $K_{W/G}$ for the *n*-alkane oxidation products. COSMOtherm was also applied to estimate

$K_{W/G}$ and $K_{WIOM/G}$ at selected temperatures for 22 α-pinene oxidation products, using either structure B, ESTER_dimer and C813OOH as surrogate solvents to represent WIOM.

The salting-out effect on aqueous phase/gas phase partitioning was quantified by estimating a compound specific Setschenow coefficient K_S in ammonium sulphate solution using a ppLFER by Wang et al. (submitted) and then calculating a salt solution/gas phase equilibrium partition coefficient $K_{S/G}$ using:

$$\log K_{S/G} = \log K_{W/G} - [salt]K_S \qquad \text{eq. 10}$$

where [salt] is the molar concentration of ammonium sulphate in aqueous salt solution, which was varied between 0 and 6.6 M, the latter corresponding to a supersaturated solution as may be encountered in aqueous aerosol (Zuend and Seinfeld, 2012).

All estimated partitioning data are given in an Excel© file in the Supplement.

3 Results

3.1 Placing the SOA Compounds in the Chemical Partitioning Space

Figure 2 shows the location of the SOA compounds in the partitioning space. The chemicals are located based on their $K_{W/G}$ and $K_{WIOM/G}$ at 15 °C estimated with SPARC using structure B as a surrogate for WIOM and assuming no salting out effect. Differently coloured markers designate compounds derived from different precursors.

Comparing a chemical's location relative to the thresholds for dominant phase distribution, that were introduced in Fig. 1 and are integrated into Fig. 2, allows us to graphically deduce its phase distribution behaviour. It is apparent that the oxidation products of *n*-alkanes (blue dots in Fig. 2) generally have higher log $K_{WIOM/G}$ and lower $K_{W/G}$ than the oxidation products of terpenes and aromatic hydrocarbons and therefore tend to have a higher affinity for the WIOM phase than the aqueous phase when they become insufficiently volatile to remain in the gas phase. Lower $K_{W/G}$ values of the products formed from α- and β-pinene and d-limonene (green and red dots in Fig. 2, respectively) means that they cluster around the line separating predominant partitioning to WIOM and aqueous phase. The graphical analysis also suggests that most of the oxidation products of the mono-aromatic hydrocarbons identified by Forstner et al. (1997) (yellow dots in

Fig. 2) are too volatile to notably contribute to organic aerosol formation under most atmospheric conditions. SOA formed during the oxidation of monoaromatics (Ng et al. 2007, Wyche et al. 2009) is therefore unlikely to be made up of the substances identified in Forstner et al. (1997) and displayed in Fig. 2. An exception is a cloud, where many oxidation products from all types of precursors could be expected to partition substantially into cloud water.

Figure 2 does not show the position of small water-soluble compounds, such as the C2 and C3 compounds typically associated with aqueous SOA (e.g. glyoxal, methylglyoxal, oxalic acid, etc.) (Lim et al., 2010). The distribution of these compounds between gas and particle phase is often strongly influenced by hydration and possibly other reactions in the aqueous phase (Ip et al., 2009, Volkamer et al., 2009, Kampf et al., 2013) leading to "effective" partition coefficients that are orders of magnitude higher than estimated ones (e.g. Rossignol et al., 2012). Furthermore, many smaller acids are expected to ionize substantially under the pH condition prevailing in aerosol water and the $K_{W/G}$ predicted for the neutral form may often underestimate the preference for the aqueous phase. Following Volkamer et al. (2009), it would be possible to locate these compounds in the partitioning space based on their "effective" partition coefficients, as long as these can be reliably derived.

Figure 3 is identical to Fig. 2, except that now the markers designating the SOA compound are coloured based on their average carbon oxidation state (OS_C) and number of carbons (n_C). Figure S1 in the supplementary material displays a similar plot based on the compounds' oxygen:carbon ratio (O:C). These plots allow us to relate a chemical's location in the partitioning space with its molecular size and oxidation state. An increase in n_C corresponds to a shift to the right in the chemical partitioning space, i.e. larger chemicals have a higher affinity for the WIOM phase relative to the gas phase. Increasing n_C in the form of methylene groups, on the other hand, hardly affects a chemical's relative affinity for water and the gas phase, i.e. an additional $–CH_2–$ decreases vapour pressure and water solubility almost to the same extent. *n*-alkane oxidation products that only deviate in their chain length are arranged along lines that are parallel to the x-axis (Fig. 3A). If a series of compound varies in n_C because of additional aromatic carbons, such as the polycyclic aromatic hydrocarbons, the increase in $K_{WIOM/G}$ is accompanied by a smaller increase in $K_{W/G}$ (Lei and Wania, 2014). An increase in a compound's OS_C is reflected by a shift down and slightly to the right in the partitioning space, i.e. more oxidized species have a higher relative affinity for the aqueous than the WIOM and gas phase. SOA compounds' OS_C increases

largely because of the addition of oxygen containing functional group, which leads to an increase in $K_{W/G}$. The O:C ratio shows similar but less clear trends as the OS_C (Fig. S1).

3.2 Categorizing Compounds Based on Their Atmospheric Phase Distribution Behaviour

We can now classify organic compounds based on their atmospheric phase distribution behaviour. Figure 4 assigns labels to different zones of the chemical partitioning space. Based on their tendency to partition to condensed phases, compounds are classified as volatile (V), semi-volatile (SV), low volatile (LV), and extremely low volatile (ELV). Based on their preferred condensed phase, compounds are further categorised as hydrocarbon-like (HOC, preference for WIOM), oxygenated (OOC, no obvious preferred condensed phase), and water-soluble (WSOC, preference for aqueous phase).

At equilibrium less than 1% of a VOC (log $K_{WIOM/G}$ and log $K_{W/G} < 8$) is predicted to be in the condensed phase even under high OAL conditions (100 μg/m^3). A chemical is presumed to be a LVOC (log $K_{WIOM/G}$ and log $K_{W/G} > 14$), if less than 1% is predicted to be in the gas phase even under low OAL conditions (1 μg/m^3). SVOCs ($8 <$ log $K_{WIOM/G}$ or log $K_{W/G} < 14$) are in between VOCs and LVOCs. Similarly, at equilibrium less than 1 % of a HOC (log $K_{WIOM/W} > 3$) partitions into the aqueous phase, even under low OAL conditions, and less than 1 % of a WSOC (log $K_{WIOM/W} < -3$) partitions into the WIOM phase, even if OAL is high. OOCs fall in between HOCs and WSOCs ($-3 <$ log $K_{WIOM/W} < 3$). Because of the widely different LWC, SV-WSOCs occupy a different part of the partitioning space under clear conditions and in a cloud. Whereas chemicals with a log $K_{W/G} < 8$ are VOCs at low RH, that threshold shifts to a log $K_{W/G}$ of 3.5 within a cloud.

The nomenclature in Fig. 4 builds upon previous classifications of SOA compounds (Kroll et al., 2011, Donahue et al., 2012). In particular, the aerosol mass spectrometry community uses HOA and OOA to refer to hydrocarbon-like and oxygenated organic aerosol. However, the use of the terms here may not always be entirely congruous with previous efforts. For example, our definition of SVOCs comprises some of the compounds that would be called intermediate volatility organic compounds (IVOCs) and LVOCs by Donahue et al. (2012).

Figure 4 reveals that higher generation oxidation products of monoterpenes and mono-aromatic hydrocarbons fall mostly into the SV-OOC category in the centre of the partitioning space, indicating that they may partition to a significant extent into gas, aqueous and WIOM phase depending on the prevailing atmospheric conditions. This also means that their exact placement in the space is important, because it will affect the predicted phase distribution. So far, we have used a single point to designate a chemical's location in the partitioning space, although this location is variable for two primary reasons: prediction uncertainty and environmental variability. In the next two sections, we will explore these sources of variability in more detail.

3.3 Influence of Prediction Uncertainty on Placement of *n*-Alkane Oxidation Products in the Partitioning Space

In order to evaluate the uncertainty of the placement of chemicals in the partitioning space, we sought to quantify the confidence of the $K_{WIOM/G}$ and $K_{W/G}$ predictions by comparing the results of different prediction methods. The values obtained for the partition coefficients of three *n*-alkanes (C9, C13, C17) and their oxidation products at 25 °C by ppLFER (average for four aerosol), SPARC (using structure B for WIOM), and COSMOtherm (using structure B for WIOM) are displayed in Fig. 5. The uncertainty of $K_{WIOM/G}$ had previously been explored in Wania et al. (2014) and had been found to be a composite of the uncertainty of the prediction method and the uncertainty of the conceptual approach (How well do a surrogate's solvation properties match those of the organic aerosol phase? How representative are the solvation properties of the four real aerosol types characterized by Arp et al. (2008) of those of aerosol in general?). The uncertainty of the $K_{W/G}$ is solely due to the uncertainty of the prediction method.

We use arrows to illustrate the displacement of a chemical in the partitioning space when we apply different prediction methods: the origin of each arrow is the location obtained by SPARC predictions. The end of the blue and red arrow is the location obtained using ppLFERs and COSMOtherm, respectively. The length of the arrow is thus a measure of the uncertainty of the prediction (the horizontal and vertical displacement indicating the discrepancy in $K_{WIOM/G}$ and $K_{W/G}$ predictions, respectively) and arrows consistently pointing in a particular direction indicate a bias of one method relative to another.

The arrows in Fig. 5 tend to get longer when moving from the upper left to the lower right of the partitioning space, suggesting that the discrepancy between predictions becomes larger as chemicals become less volatile. This is expected as predictions for these less volatile, multi-functional chemicals involve an extrapolation from the type of chemicals for which empirical partitioning data are available and which are therefore the basis of the calibration of the ppLFER and also the SPARC method. The vertical displacements in Fig. 5 tend to be larger than the horizontal ones, indicating that the uncertainty of the $K_{W/G}$ prediction is higher than that of $K_{WIOM/G}$. Most arrows are pointing to the left, which means that SPARC predicts generally higher $K_{WIOM/G}$ than the other two methods. Most red arrows are pointing upwards, indicating that SPARC also predicts higher $K_{W/G}$ than COSMOtherm.

The uncertainty in the placement of chemicals falling into the area close to the phase transition between gas and WIOM phase is generally less than an order of magnitude for $K_{WIOM/G}$ and less than two orders of magnitude for $K_{W/G}$ (Fig. 5). The latter is generally of little consequence because the oxidation products of the *n*-alkanes are not sufficiently polar to partition to the aqueous aerosol phase, unless the LWC is very high (i.e. in a cloud). The uncertainty of $K_{WIOM/G}$ on the other hand is sufficiently large to significantly change the predicted partitioning behaviour of SV-HOCs with a log $K_{WIOM/G}$ ranging from 10 to 12. It is worthwhile, however, to reiterate Wania et al. (2014)'s observation that the prediction uncertainty in $K_{WIOM/G}$ for the *n*-alkane oxidation products is much smaller than the prediction uncertainty of saturation vapour pressure normally used to predict the phase distribution behaviour of SOA compounds.

3.4 Influence of Environmental Variability on Placement of α-Pinene Oxidation Products in the Partitioning Space

We use α-pinene oxidation products to illustrate the effect of temperature, aqueous phase salinity and WIOM phase polarity on the placement of chemicals in the partitioning space. Because it is difficult to discuss the impact of environmental variability without also considering the prediction uncertainty discussed in Sect. 3.3, we produced multiple plots using different predictions. Figures 6A and B are based on SPARC and COSMOtherm-predicted partition coefficients, respectively, and Fig. S2 in the supporting material is based on ppLFER predictions. The number of compounds with COSMOtherm predictions is smaller than for the other two methods. In these plots, three intersecting lines represent each chemical. The diagonal line

indicates the variability in the partition coefficients caused by temperature (upper left of the line is for 30 °C, lower right is for 0 °C). The vertical line designates the salting-out effect, which yields a decrease in $K_{W/G}$. The uppermost value on that line indicates the $K_{W/G}$ in a 6.6 M supersaturated solution of $(NH_4)_2SO_4$. The horizontal line indicates the range of $K_{WIOM/G}$ obtained by using different surrogate molecules to represent the WIOM phase (Fig. 6). In the case of the ppLFER-based plot (Fig. S2), the horizontal line indicates the range of values obtained by applying ppLFER equations for four different aerosols. Where the three lines intersect are the partition coefficients at 15 °C, at 0 M $(NH_4)_2SO_4$ and using structure B as a surrogate for WIOM (Fig. 6) or the average of the four ppLFER-predicted $K_{WIOM/G}$ (Fig. S2). An arrow plot (Fig. S3) further displays the discrepancy between the three sets of predictions at 15 °C and 0 M.

The lines are coloured based on the number of oxygens in the molecules, ranging from 0 (α-pinene itself) to 7 (a highly oxygenated product listed by Valorso et al., 2011). Dashed lines designate nitrated molecules. The α-pinene oxidation products fall along a band from the upper left (α-pinene itself) to the lower right (highly oxygenated products as well as dimers) of the partitioning space. Oxidation products with the same number of oxygens tend to cluster together within the partitioning space.

Differences between the prediction methods overall seem quite random and not biased (the arrows in Fig. S3 point in all sorts of directions). However, for the oxidation products with 5 and more oxygen the blue arrows point mostly to the upper right, i.e., the ppLFER prediction of $K_{WIOM/G}$ appear to be generally biased low relative to SPARC predictions and the $K_{W/G}$ appear to be biased high, i.e. ppLFER predictions favour the aqueous over the WIOM phase. For three compounds (C108OOH, C813OOH, C721CHO), the ppLFER predicted $K_{W/G}$ is much lower than the COSMOtherm predicted one (by 4.5 to 5.5 orders of magnitude), further suggesting that ppLFER are unduly favouring the aqueous phase. It is possible that the highly functionalised α-pinene products fall outside the domain of applicability of the ppLFER equations (esp. for $K_{W/G}$) and we therefore disregard the predictions displayed in Fig. S2 in the further discussion.

It is readily apparent from Fig. 6 that environmental variability in temperature, aqueous phase salinity and WIOM phase polarity can have a strong impact on the partitioning properties of the SOA compounds and therefore the placement within the partitioning space. Comparing the

length of the lines in Fig. S3 with those in Fig. 6 suggests that in most cases the effect of environmental parameter variability on chemical placement is larger than that caused by prediction uncertainty. The length of the diagonal lines indicates that temperature differences of 30 °C can change both $K_{W/G}$ and $K_{WIOM/G}$ by orders of magnitude, and the length of the vertical line demonstrates that salting-out can have a similarly large effect on $K_{W/G}$. COSMOtherm and SPARC disagree to what extent phase polarity affects $K_{WIOM/G}$: Whereas the long horizontal lines in Fig. 6A mean that SPARC predicts that $K_{WIOM/G}$ of the α-pinene oxidation products increases substantially, if the WIOM phase is more polar (i.e. when the surrogate solvent is changed from structure B to ESTER_dimer or C813OOH), the much shorter horizontal lines in Fig. 6B (and Fig. S2) indicate that COSMOtherm (and ppLFERs) predict a much more modest influence of phase polarity.

A more explicit comparison of $K_{WIOM/G}$ values obtained for different surrogate solvents (Fig. S4) shows that SPARC and COSMOtherm actually agree that the solvation properties of C813OOH and ESTER_dimer should be similar. They disagree however, to what extent the solvation properties of these two more polar surrogates deviate from those of Kalberer et al. (2004)'s structure B. The length of the horizontal lines in Fig. 6A would imply that the activity coefficients of the compounds in different organic solvents can vary by as much as four orders of magnitude, which is not very plausible. The SPARC predictions for the highly polar solvents should therefore be considered suspect, also because SPARC may fail to accurately predict partitioning into organic phases for which few empirical data for calibration are available (Stenzel et al., 2014).

The various predictions however agree in many other regards, for example with respect to the effect of temperature. Lower temperatures always shift chemical distribution to the condensed phases, and the temperature effect on $K_{W/G}$ and $K_{WIOM/G}$ is similar (i.e. the temperature lines in Fig. 6 are more or less parallel to the line designating the transition between dominant partitioning into WIOM and aqueous phase). The only exceptions are the most volatile species, such as α-pinene itself, where a drop in temperature actually leads to a small decrease in $K_{W/G.}$ The partition coefficients become more temperature dependent as they increase, i.e. the lines for the least volatile chemicals in the lower right are the longest. This implies that the effect of temperature on partitioning is stronger for the higher generation oxidation products and is due to the well-known linear correlation between the logarithm of a partition coefficient and the

enthalpy of phase transfer (Goss and Schwarzenbach, 1999). The vertical lines, on the other hand, decrease in length with increasing oxygenation, i.e., the salting-out effect is weaker for the higher generation oxidation products. This is because Setschenow coefficients are smaller for more polar substances (Endo et al., 2012, Wang et al., 2014).

By comparing the placement of chemicals in Fig. 6 with the boundaries of dominant phase distribution introduced in Fig. 1, we can graphically predict the phase distribution behaviour of α-pinene oxidation products under different conditions (Figs. 6A and 6B display the boundaries for LWC typical for aerosol and clouds, respectively). At the low LWC typical of aerosol (Fig. 6A) products with four oxygen atoms are starting to contribute to the condensed phase, especially at higher OALs and lower temperature. Products with five and more oxygen atoms are already predicted to have only minor fractions in the gas phase, falling close to the boundary between aqueous and WIOM phase. The salting-out effect likely assures that those α-pinene oxidation products would be found mostly in the WIOM phase. Products with seven and more oxygen atoms (i.e. the ELVOCs observed as major products of α-pinene oxidation in the field by Ehn et al. (2014)) would clearly no longer be in the gas phase under any conditions.

The partitioning space analysis also suggests that under the high LWC conditions typical of a cloud (Fig. 6B) oxidation products of α-pinene with three and even only two oxygen would partition strongly into the aqueous condensed phase, also because the salting-out effect would not longer be active. This incidentally highlights why an analysis of phase partitioning that ignores liquid water in the atmosphere can lead to erroneous conclusions, especially in the presence of clouds. The red outlines in Figs. 6A and 6B designate the region where chemicals fall whose contribution to SOA formation would not be taken into account, if the aqueous phase were ignored. At low LWC typical of aerosol (solid red outline), this applies to few, if any, oxidation products, but at high LWC typical of clouds (dashed red outline), a very large number of oxidation products would remain in the gas phase. This appears to be in agreement with Pankow et al. (2013), who predicts "significant RH-induced enhancement of organic particulate matter condensation" in the α-pinene/ozone system.

Incidentally, none of the α-pinene oxidation products are predicted to partition notably into WIOM at high LWC typical of clouds (Fig. 6B). This probably means that unless there is another

source of WIOM to the atmosphere, a single mostly aqueous aerosol phase would form under such conditions.

We stress that there are other reasons why a chemical's location may depend on environmental conditions. For example, some SOA compounds are acids with pK_A values in the pH range encountered in the aqueous phase of aerosol and cloud droplets, i.e. they can be expected to be ionized to some degree. Ionization increases $K_{W/G}$ relative to the value that is estimated by the prediction methods for the protonated form of the acids. It also means that $K_{W/G}$, and therefore the placement in the partitioning space depends on the pH of the aqueous phase.

3.5 Illustrating Displacement within the Partitioning Space Caused by Chemical Transformations

So far, the SOA compounds have been considered in isolation and not as part of a chemical reaction sequence. Figure 7 shows the oxidation products of the C17 *n*-alkane linked by arrows designating the chemical reactions elucidated by Lim and Ziemann (2005). Like the α-pinene oxidation products in Fig. 6, the oxidation products fall along a band that starts at the precursor VOC in the upper left and extends to the lower right of the partitioning space. Remarkably, the slope of that band and even the extent of its broadening toward the lower right is very similar for C17 (and by inference all *n*-alkanes) and α-pinene. This similarity is not really surprising, as in both cases hydroxyl, carbonyl, peroxyl, nitrate, and carboxylic acid functional groups are being added to an aliphatic compound. Hodzic et al (2014) also noted that the relationships between effective Henry's law constant and saturation concentration were similar for the products of different precursors.

The slope of these bands of compounds within the partitioning space suggests that on average such functionalization roughly increases the $K_{W/G}$ by two log units for every log unit increase in log $K_{WIOM/G}$, i.e. the addition of functional groups increases the affinity for the aqueous phase more rapidly than the affinity for the WIOM phase. Incidentally, this is different from what Hodzic et al. (2014) noted for the oxidation products of different precursors: for a one log unit change in saturation concentration, the effective Henry's law constant only changed by 0.5 to 0.9 log units. Whether the functionalization of a precursor VOC ends up generating compounds that prefer the WIOM or the aerosol aqueous phase thus depends to some extent on the location of

564 that precursor in the partitioning space. The lower the $K_{W/G}$ and the higher the $K_{WIOM/G}$ of a
565 precursor, the more likely it is to generate oxidation products that favour the WIOM phase.

566 The broadening of the band is due to different changes in $K_{W/G}$ and $K_{WIOM/G}$ occurring upon the
567 addition of different functional groups. According to Lim and Ziemann (2005), the first few steps
568 of the oxidation of *n*-alkanes by OH in the presence of NO_X, involves primarily five types of
569 transformations. The displacement within the partitioning space caused by these transformations
570 is depicted in Fig. 8.

571 As expected from the general trend toward the lower right seen in Fig. 7, the addition of
572 functional groups to the aliphatic chain increases both $K_{WIOM/G}$ and $K_{W/G}$, i.e., arrows pointing to
573 the lower right represent the reaction steps. The exception is the formation of cyclical
574 dihydrofurans from δ-hydroxycarbonyls, which leads to a displacement in the opposite direction,
575 i.e. to a more volatile substance. Size and direction of the displacement in the partitioning space
576 depends on the functional groups being added. The addition of oxygen-containing groups such as
577 hydroxyl, carbonyl, and carboxylester, increases $K_{W/G}$ more than $K_{WIOM/G}$, i.e. the mean vertical
578 displacement is generally more than double the mean horizontal displacement. The addition of
579 nitrate, on the other hand, leads to about equal displacement in the vertical and horizontal
580 direction, i.e., causes $K_{W/G}$ and $K_{WIOM/G}$ to increase by the same extent. This incidentally explains
581 why nitrated compounds (represented by broken lines in Fig. 6A) and especially di-nitrated
582 compounds (UR37, UR38, UR39, UR41, UR42 in Fig. 7) tend to fall on the right side of the
583 band of oxidation products, whereas those without nitrate substitutions (RP20, RP21, UR36 in
584 Fig. 7) on the left. This implies that nitration increases the affinity for WIOM more than the
585 addition of carbonyls, hydroxyls and carboxylester does. This is in agreement with Hodzic et al.
586 (2014), who noted that products formed during low NO_x conditions are predicted to be more
587 soluble.

588 To which compound a functional group is being added often does not seem to matter much (i.e.
589 the arrows within each panel of Fig. 8 are of similar length and point in a similar direction). In
590 particular the alkyl-chain length plays a limited role (blue and green arrows are very similar).
591 However, the displacement caused by the addition of nitrate is different for different compounds.
592 For example, nitration of the dihydrofuran leads to a larger change in $K_{WIOM/G}$ and $K_{W/G}$ (longer

arrows) than nitration of the aliphatic chain. The addition of a second nitrate leads to a smaller increase in $K_{W/G}$ (arrows point more to the right) than the first nitrate.

To obtain a broader set of displacements caused by chemical transformations, we also looked at the functionalization occurring during oxidation of aromatic hydrocarbons (Fig. S5). This analysis confirmed that the addition of oxygen-containing functional groups again increases both $K_{WIOM/G}$ and $K_{W/G}$, with the latter increasing more rapidly, i.e., the vertical displacement being slightly larger than the horizontal one. The displacement is increasing from carbonyl to hydroxyl to carboxyl groups (i.e. arrows are getting longer in Fig. S5), whereby the sum of the displacements caused by a carbonyl and a hydroxyl group is larger than the displacement caused by the addition of a carboxyl group. Similar to the addition of a nitrate group to the *n*-alkane oxidation products (Fig. 8), the addition of a nitro-group to a mono-aromatic hydrocarbon increases $K_{WIOM/G}$ and $K_{W/G}$ to the same extent, i.e., horizontal and vertical displacements are very similar (Fig. S5). Increasing the size of a mono-aromatic compound through the addition of methyl- and methylene-groups has only a very minor effect on the placement in the partitioning space, increasing $K_{WIOM/G}$ only slightly and $K_{W/G}$ hardly at all (Fig. S5).

In the case of –OH and $–NO_2$ addition to a mono-aromatic hydrocarbon, the displacement in the partitioning space can be strongly dependent on the type of functional groups already present in the molecule. The difference in the change in $K_{WIOM/G}$ and $K_{W/G}$ occurring upon the addition of –OH directly to the aromatic ring or to an existing carbonyl group (i.e. conversion of benzaldehyde to benzoic acid) is relatively small (Fig. 9A). On the other hand, the effect on partitioning upon the addition of –OH is much diminished, if the hydroxyl can form intramolecular hydrogen bonds with an existing carbonyl or nitro group (Fig. 9A). The widely different shift in the partitioning space occurring upon the addition of a nitro group (Fig. 9B) further confirms that it is not merely the presence of existing polar functional groups in the molecules that matters, but whether those functional groups are in a position to form intramolecular hydrogen bonds with the $–NO_2$. For example, SPARC predicts that the addition of $–NO_2$ at the ortho-position to an existing –OH hardly changes the partitioning properties at all, whereas addition at the para-position increases both $K_{WIOM/G}$ and $K_{W/G}$ by more than three orders of magnitude (Fig. 9B).

So far, we have only considered transformations that lead to functionalization of an aliphatic or aromatic carbon structure. Dimerisation reactions in the condensed phase are also believed to play a role in SOA formation. Figure 10 shows the displacements caused by various dimerisation reactions proposed for the ozonolysis reaction products of α-pinene by Camredon et al. (2010). The partition coefficients of both monomers and dimers at 15 °C in this plot were estimates with SPARC, although it is possible that the very large dimer molecules fall outside of the domain of applicability of SPARC.

Dimer formation increases both $K_{WIOM/G}$ and $K_{W/G}$ and thus leads to a displacement to the lower right (Fig. 10). The overall effect of dimerisation is the conversion of semivolatile organic compounds into low and extremely low volatility compounds. The extent and the direction of displacement appear to depend on the type of reaction, with hemiacetal and peroxyhemiacetal formation causing the largest overall displacement (longest arrows in Fig. 10) and the largest increase in $K_{W/G}$ relative to $K_{WIOM/G}$ (steepest incline of the arrows in Fig. 10). Most dimerisations however are predicted to increase $K_{WIOM/G}$ and $K_{W/G}$ to the same extent.

4 Discussion

One main application of the chemical partitioning space maps introduced here is the possibility to visualise and therefore easily compare the impact of a wide variety of factors on SOA formation. For example, it allows for a direct comparison of the uncertainty of the prediction of partition coefficients with the impact of atmospheric variability on these coefficients. It facilitates a comparison of the direction and size of the effects of temperature, salinity and organic phase polarity on the partitioning behaviour of different SOA compounds. The change in partitioning behaviour occurring upon dimerisation can be compared with that of adding a hydroxyl or a nitrate functional group. Because everything is displayed within the same two-dimensional framework, even very different factors can be assessed comparatively: prediction uncertainty can be compared with the effect of a change in OAL or LWC on partitioning, the effect of a chemical reaction, or the effect of a change in temperature and ammonium sulphate concentration.

This suitability for comparative visualisation can serve to aid in the understanding of dynamic processes, where several of the factors affecting phase distribution are changing at the same time. For example, during a photochemical smog episode, or during a chamber experiment, the

652 precursor VOCs become oxidized and with increasing functionalization - and eventually also
653 dimerisation - the oxidation products partition increasingly into the condensed phase (i.e. they
654 move to the lower right of the partitioning space) (Fig. 11). As a result, the OAL is increasing
655 causing the vertical threshold separating dominant phase distribution into gas and WIOM phase
656 to move to the left (Fig. 11). This implies that with ongoing SOA formation, more and more
657 volatile chemicals become available for partitioning to the WIOM. Overall, the changes in
658 partitioning behaviour caused by the chemical processes are considerably larger than the shift in
659 the threshold caused by the increase in OAL (Fig. 11).

660 Similarly, during cloud droplet formation a large upward shift in the horizontal threshold
661 between dominant phase distribution into water and gas phase coincides with a downward shift
662 in the position of SOA compounds in the partitioning space, as salts become diluted and the
663 salting out effect becomes negligible. Another example is the dilution of tail pipe emissions,
664 which is accompanied by a rapid decrease in both OAL and temperature, having opposing effects
665 on the partitioning between gas and WIOM phase (May et al., 2013).

666 Another application of the partitioning space is the identification and prioritization of data gaps.
667 The maps graphically highlight the factors and effects that matter and for which compounds they
668 matter. They provide guidance to distinguish processes and parameters that need to be known
669 more accurately and more precisely from those with tolerable uncertainty. For example, there is
670 little to be gained from improved quantitative knowledge of the partitioning properties of VOCs
671 and ELVOCs. On the other hand, resolving the disagreement of the prediction methods with
672 respect to the size of the effect of WIOM phase polarity on $K_{WIOM/G}$ should be a priority. Also
673 important is improving quantitative knowledge of $K_{W/WIOM}$ and Setschenow coefficients (K_S) of
674 the SV-OOCs and LV-OOCs and of $K_{W/G}$ and K_S of substances falling in the red outlines of Fig.
675 6.

676 The chemical partitioning plots provide a new integrated perspective that looks at the formation
677 of WIOM and aqueous phase SOA at the same time. The plots suggest that many oxidation
678 products (including dimers formed by condensed phase reactions) fall into the transition area
679 between WIOM and aqueous phase in the lower right of the partitioning space. This is because
680 the WIOM and aqueous phase volumes are actually quite similar (LWC and OAL are within the
681 same order of magnitude under clear cloud conditions) and because the highly functionalised

oxidation products are predicted to have a reasonably similar affinity for WIOM and water (i.e. $0.01 < K_{WIOM/W} < 100$). Often it may be the presence of inorganic salts and the resulting salting-out effect that decides whether an SOA compound will be in the WIOM or aqueous phase. Temperature, incidentally, will have little direct impact in this regard, because $K_{WIOM/W}$ is hardly dependent on temperature (the lines in Fig. 6 are parallel to the dividing line between dominant phase distribution to WIOM and aqueous phase). Temperature changes, of course, impact relative humidity and thus LWC and can have an indirect effect on the distribution between WIOM and water. Does it matter whether an oxidation product is in the WIOM or the aqueous phase, as long as it is contributing to the OAL? The relative volumes of WIOM and aqueous phase vary in the atmosphere. For example, the liquid water content in wet aerosol is regionally different, driven largely by sulphate concentrations (Carlton et al., 2013). Therefore, partitioning between the two condensed phases and the value of $K_{W/WIOM}$ is important for predicting SOA formation, composition and yield. Also, the occurrence and kinetics of condensed phase reactions that oxidation products may undergo, such as dimerisations or reactions with sulphate are likely to be different in the WIOM and aqueous phase.

Several 2-dimensional property spaces have been advocated for describing organic aerosol characteristics (Pankow and Brasanti, 2009, Kroll et al., 2011, Cappa and Wilson, 2012), the 2D VBS by Donahue et al. (2011, 2012) using saturation concentration and O:C ratio (or OS_C) being the most conspicuous. One of the key shortcomings of the 2D VBS approach is, that it "does not allow consideration of water uptake or variable partition coefficients" (Pankow et al., 2013). Donahue et al. (2012) actually mention this when introducing the 2D-VBS: "The formulation so far does not address the role of water. […] However, because water can be a dominant component, and therefore its unique properties are more likely to challenge the mean-field assumption, it is likely that explicit treatment of humidity effects will be required." Here we have presented what essentially amounts to an alternative 2-dimensional approach to SOA characterization based on partition coefficients from gas phase into WIOM and water. This approach includes partitioning into an aqueous phase and directly addresses one of the key issues that atmospheric modelers of SOA formation aim to address: which fraction of the products formed from the oxidation of VOCs will end up in the SOA after equilibration under different atmospheric conditions. We could imagine that it is possible to develop parameterizations of the chemical partitioning space introduced here, which – combined with gas phase concentrations of

sets of compounds with comparable partitioning properties – are suitable for implementation in atmospheric models seeking to explicitly describe the formation of SOA.

Acknowledgements

The authors acknowledge financial support from the Natural Sciences and Engineering Research Council of Canada (NSERC).

References

Arp, H. P. H. and Goss, K. U.: Ambient gas/particle partitioning. 3. Estimating partition coefficients of apolar, polar, and ionizable organic compounds by their molecular structure. Environ. Sci. Technol., 43, 1923-1929, 2009.

Arp, H. P. H., Schwarzenbach, R. P., and Goss, K. U.: Ambient gas/particle partitioning. 2: The influence of particle source and temperature on sorption to dry terrestrial aerosols, Environ. Sci. Technol., 42, 5951–5957, 2008.

Bertram, A. K., Martin, S. T., Hanna, S. J., Smith, M. L., Bodsworth, A., Chen, Q., Kuwata, M., Liu, A, You, Y., and S. R. Zorn, S. R.: Predicting the relative humidities of liquid-liquid phase separation, efflorescence, and deliquescence of mixed particles of ammonium sulfate, organic material, and water using the organic-to-sulfate mass ratio of the particle and the oxygen-to-carbon elemental ratio of the organic component. Atmos. Chem. Phys., 11, 10995-11006, 2011.

Camredon, M., Hamilton, J. F., Alam, M. S., Wyche, K. P., Carr, T., White, I. R., Monks, P. S., Rickard, A. R., and Bloss, W. J.: Distribution of gaseous and particulate organic composition during dark α-pinene ozonolysis. Atmos. Chem. Phys., 10, 2893–2917, 2010.

Cappa, C. D. and Wilson, K. R.: Multi-generation gas-phase oxidation, equilibrium partitioning and the formation and evolution of secondary organic aerosol. Atmos. Chem. Phys. 12, 9505-9528, 2012.

Carlton, A. G. and Turpin, B. J.: Particle partitioning potential of organic compounds is highest in the Eastern US and driven by anthropogenic water. Atmos. Chem. Phys. 13, 10203-10214, 2013.

Chen, J. J. and Griffin, R. J.: Modeling secondary organic aerosol formation from oxidation of alpha-pinene, beta-pinene, and d-limonene. Atmos. Environ., 39, 7731-7744, 2005.

741 Ehn, M., Thornton, J. A., Kleist, E., Sipilä, M., Junninen, H., Pullinen, I., Springer, M., Rubach,
742 F., Tillmann, R., Lee, B., Lopez-Hilfiker, F., Andres, S., Acir, I.-H., Rissanen, M., Jokinen, T.,
743 Schobesberger, S., Kangasluoma, J., Kontkanen, J., Nieminen, T., Kurtén, T., Nielsen, L. B.,
744 Jørgensen, S., Kjaergaard, H. G., Canagaratna, M., Dal Maso, M., Berndt, T., Petäjä, T., Wahner,
745 A., Kerminen, V.-M., Kulmala, M., Worsnop, D. R., Wildt, J., and Mentel, T.F.: A large source
746 of low-volatility secondary aerosol. Nature, 506, 476-479, 2014.

747 Endo, S., Pfennigsdorff, A., and Goss, K.-U.: Salting-out effect in aqueous NaCl solutions:
748 Trends with size and polarity of solute molecules. Environ. Sci. Technol., 46, 1496–1503, 2012.

749 Donahue, N. M., Robinson, A. L., Stanier, C. O., and Pandis, S.N.: Coupled partitioning,
750 dilution, and chemical aging of semivolatile organics. Environ. Sci. Technol., 40, 2635-2643,
751 2006.

752 Donahue, N. M., Epstein, S. A., Pandis, S. N., and Robinson, A. L.: A two-dimensional volatility
753 basis set: 1. organic-aerosol mixing thermodynamics. Atmos. Chem. Phys., 11, 3303-3318, 2011.

754 Donahue, N. M., Kroll, J. H., Pandis, S. N., and Robinson, A. L.: A two-dimensional volatility
755 basis set: 2: Diagnostics of organic-aerosol evolution. Atmos. Chem. Phys., 12, 615-634, 2012.

756 Forstner, H. J. L., Flagan, R. C., and Seinfeld, J. H.: Secondary organic aerosol from the
757 photooxidation of aromatic hydrocarbons: molecular composition. Environ. Sci. Technol. 31,
758 1345-1358, 1997.

759 Goss, K.-U. and Schwarzenbach, R. P.: Empirical prediction of heats of vaporization and heats
760 of adsorption of organic compounds. Environ. Sci. Technol., 33, 3390-3393, 1999.

761 Goss, K.-U.: Prediction of the temperature dependency of Henry's law constant using poly-
762 parameter linear free energy relationships. Chemosphere, 64, 1369–1374, 2006.

763 Hallquist, M., Wenger, J. C., Baltensperger, U., Rudich, Y., Simpson, D., Claeys, M., Dommen,
764 J., Donahue, N. M., George, C., Goldstein, A. H., Hamilton, J. F., Herrmann, H., Hoffmann, T.,
765 Iinuma, Y., Jang, M., Jenkin, M. E., Jimenez, J. L., Kiendler-Scharr, A., Maenhaut, W.,
766 McFiggans, G., Mentel, Th. F., Monod, A., Prévôt, A. S. H., Seinfeld, J. H., Surratt, J. D.,
767 Szmigielski, R., and Wildt J.: The formation, properties and impact of secondary organic aerosol:
768 current and emerging issues. Atmos. Chem. Phys., 9, 5155-5236, 2009.

769 Heald, C. L., Kroll, J. H., Jimenez, J. L., Docherty, K. S., DeCarlo, P. F., Aiken, A. C., Chen, Q.,
770 Martin, S. T., Farmer, D. K. and Artaxo, P.: A simplified description of the evolution of organic
771 aerosol composition in the atmosphere. Geophys. Res. Lett. 37, L08803,
772 DOI: 10.1029/2010GL042737, 2010.

773 Hilal, S. H., Carreira, L. A., and Karickhoff, S. W.: Prediction of the solubility, activity
774 coefficient, gas/liquid and liquid/liquid distribution coefficients of organic compounds, QSAR &
775 Combinatorial Science, 23, 709–720, 2004.

776 Hodzic, A., Aumont, B., Knote, C., Madronich, S. and Tyndall, G.: Volatility dependence of
777 Henry's law constants of condensable organics: Application to estimate depositional loss of
778 secondary organic aerosols, Geophys. Res. Lett., 41, 4795-4804, doi:10.1002/2014GL060649,
779 2014.

780 Ip, H. S. S., Huang, X. H. H., and Yu, J. Z.: Effective Henry's law constants of glyoxal,
781 glyoxylic acid, and glycolic acid. Geophys. Res. Lett., 36, L01802, doi:10.1029/2008GL036212,
782 2009.

783 Isaacman, G., Worton, D. R., Kreisberg, N. M., Hennigan, C. J., Teng, A. P., Hering, S. V.,
784 Robinson, A. L., Donahue, N. M. and Goldstein, A. H.: Understanding evolution of product
785 composition and volatility distribution through in-situ GC x GC analysis: a case study of
786 longifolene ozonolysis. Atmos. Chem. Phys., 11, 5335-5346, doi:10.5194/acp-11-5335-2011,
787 2011

788 Jimenez, J. L., Canagaratna, M. R., Donahue, N. M., Prevot, A. S., Zhang, Q., Kroll, J. H.,
789 DeCarlo, P. F., Allan, J. D., Coe, H., Ng, N. L., Aiken, A. C., Docherty, K. S., Ulbrich, I. M.,
790 Grieshop, A. P., Robinson, A. L., Duplissy, J., Smith, J. D., Wilson, K. R., Lanz, V. A., Hueglin,
791 C., Sun, Y. L., Tian, J., Laaksonen, A., Raatikainen, T., Rautiainen, J., Vaattovaara, P., Ehn, M.,
792 Kulmala, M., Tomlinson, J. M., Collins, D. R., Cubison, M. J., Dunlea, E. J., Huffman, J. A.,
793 Onasch, T. B., Alfarra, M. R., Williams, P. I., Bower, K., Kondo, Y., Schneider, J., Drewnick, F.,
794 Borrmann, S., Weimer, S., Demerjian, K., Salcedo, D., Cottrell, L., Griffin, R., Takami, A.,
795 Miyoshi, T., Hatakeyama, S., Shimono, A., Sun, J. Y., Zhang, Y. M., Dzepina, K., Kimmel, J.
796 R., Sueper, D., Jayne, J. T., Herndon, S. C., Trimborn, A. M., Williams, L. R., Wood, E. C.,
797 Middlebrook, A. M., Kolb, C. E., Baltensperger, U., and Worsnop, D. R.: Evolution of organic
798 aerosols in the atmosphere. Science, 326, 1525-1529, 2009.

799 Jordan, C. E., Ziemann, P. J., Griffin, R. J., Lim, Y. B., Atkinson, R., and Arey, J.: Modeling
800 SOA formation from OH reactions with C-8-C-17 n-alkanes. Atmos. Environ., 42, 8015-8026,
801 2008.

802 Kalberer, M., Paulsen, D., Sax, M., Steinbacher, M., Dommen, J., Prevot, A. S. H., Fisseha, R.,
803 Weingartner, E., Frankevich, V., Zenobi, R., and Baltensperger, U.: Identification of polymers as
804 major components of atmospheric organic aerosols. Science, 303, 1659-1662, 2004.

805 Kampf, C. J., Waxman, E. M., Slowik, J. G., Dommen, J., Pfaffenberger, L., Praplan, A. P.,
806 Prevot, A. S. H., Baltensperger, U., Hoffmann, T., and Volkamer, R.: Effective Henry's law
807 partitioning and the salting constant of glyoxal in aerosols containing sulfate. Environ. Sci.
808 Technol., 47, 4236-4244, 2013.

809 Koop, T., Bookhold, J., Shiraiwa, M., and Poeschl, U.: Glass transition and phase state of
810 organic compounds: dependency on molecular properties and implications for secondary organic
811 aerosols in the atmosphere. Phys. Chem. Chem. Phys., 13, 19238-19255, 2011.

812 Kroll, J. H., Donahue, N. M., Jimenez, J. L., Kessler, S. H., Canagaratna, M. R., Wilson, K. R.,
813 Altieri, K. E., Mazzoleni, L. R., Wozniak, A. S., Bluhm, H., Mysak, E. R., Smith, J. D., Kolb, C.
814 E., and Worsnop, D. R.: Carbon oxidation state as a metric for describing the chemistry of
815 atmospheric organic aerosol. Nature Chemistry, 3, 133-139, 2011.

816 Lei, Y. D. and Wania, F.: Is rain or snow a more efficient scavenger of organic chemicals?
817 Atmos. Environ., 38, 3557-3571, 2004.

818 Lim, Y. B. and Ziemann P. J.: Products and mechanism of secondary organic aerosol formation
819 from reactions of n-alkanes with OH radicals in the presence of NO_X. Environ. Sci. Technol., 39,
820 9229-9236, 2005.

821 Lim, Y. B., Tan, Y., Perri, M. J., Seitzinger, S. P., and Turpin, B. J.: Aqueous chemistry and its
822 role in secondary organic aerosol (SOA) formation. Atmos. Chem. Phys., 10, 10521–10539,
823 2010.

824 May, A. A., Presto, A. A., Hennigan, C. J., Nguyen, N. T., Gordon, T. D., and Robinson, A. L.:
825 Gas-particle partitioning of primary organic aerosol emissions: 1. Gasoline vehicle exhaust.
826 Atmos. Environ., 77, 128-139, 2013.

827 Mikhailov, E., Vlasenko, S., Martin, S. T., Koop, T., and Poeschl, U.: Amorphous and crystalline
828 aerosol particles interacting with water vapor: Conceptual framework and experimental evidence
829 for restructuring, phase transitions and kinetic limitations. Atmos. Chem. Phys., 9, 9491-9522,
830 2009.

831 Ng, N. L., Kroll, J. H., Chan, A. W. H., Chhabra, P. S., Flagan, R. C. and Seinfeld, J. H.:
832 Secondary organic aerosol formation from m-xylene, toluene, and benzene. Atmos. Chem. Phys.,
833 7, 3909-3922, doi:10.5194/acp-7-3909-2007, 2007.

834 Pankow, J. F.: Gas/particle partitioning of neutral and ionizing compounds to single and multi-
835 phase aerosol particles. 1. Unified modeling framework. Atmos. Environ. 37, 3323-3333, 2003.

836 Pankow, J. F. and Barsanti, K. C.: The carbon number-polarity grid: a means to manage the
837 complexity of the mix of organic compounds when modeling atmospheric organic particulate
838 matter. Atmos. Environ., 43, 2829-2835, 2009.

839 Pankow, J. F., Niakan, N., and Asher, W. E.: Combinatorial variation of structure in
840 considerations of compound lumping in one- and two-dimensional property representations of
841 condensable atmospheric organic compounds. 1. Lumping by 1-D volatility with n_C fixed.
842 Atmos. Environ., 80, 172-183, 2013.

843 Perraud, V., Bruns, E. A., Ezell, M. J., Johnson, S. N., Yu, Y., Alexander, M. L., Zelenyuk, A.,
844 Imre, D., Chang, W. L., Dabdub, D., Pankow, J. F., and Finlayson-Pitts, B. J.: Nonequilibrium
845 atmospheric secondary organic aerosol formation and growth. Proc. Nat. Acad. Sci. US, 109,
846 2836-2841, 2012.

847 Rossignol, S., Chiappini, L., Perraudin, E., Rio, C., Fable, S., Valorso, R., and Doussin, J. F.:
848 Development of a parallel sampling and analysis method for the elucidation of gas/particle
849 partitioning of oxygenated semi-volatile organics: a limonene ozonolysis study. Atmos. Meas.
850 Tech., 5, 1459–1489, 2012.

851 Saleh, R., Donahue, N. M., and Robinson, A. L.: Time scales for gas-particle partitioning
852 equilibration of secondary organic aerosol formed from alpha-pinene ozonolysis. Environ. Sci.
853 Technol., 47, 5588-5594, 2013.

Shilling, J. E., Chen, Q., King, S. M., Rosenoern, T., Kroll, J. H., Worsnop, D. R., DeCarlo, P. F., Aiken, A. C., Sueper, D., Jimenez, J. L., and Martin, S.T.: Loading-dependent elemental composition of alpha-pinene SOA particles. Atmos. Chem. Phys., 9, 771-782, 2009.

Shiraiwa, M., Zuend, A., Bertram, A. K., and Seinfeld, J. H.: Gas–particle partitioning of atmospheric aerosols: interplay of physical state, non-ideal mixing and morphology. Phys. Chem. Chem. Phys., 15, 11441-11453, 2013.

Song, M., Marcolli, C., Krieger, U. K., Zuend, A., and Peter, T.: Liquid-liquid phase separation and morphology of internally mixed dicarboxylic acids/ammonium sulfate/water particles. Atmos. Chem. Phys. 12, 2691-2712, 2012.

Stenzel, A., Goss, K.-U., and Endo, S.: Prediction of partition coefficients for complex environmental contaminants: Validation of COSMOtherm, ABSOLV, and SPARC. Environ. Toxicol. Chem., 33, 1537-1543, 2014.

Valorso, R., Aumont, B., Camredon, M., Raventos-Duran, T., Mouchel-Vallon, C., Ng, N. L., Seinfeld, J. H., Lee-Taylor, J., and Madronich, S.: Explicit modelling of SOA formation from α-pinene photooxidation: sensitivity to vapour pressure estimation. Atmos. Chem. Phys., 11, 6895-6910, 2011.

Virtanen, A., Joutsensaari, J., Koop, T., Kannosto, J., Yli-Pirila, P., Leskinen, J., Makela, J. M., Holopainen, J. K., Poschl, U., Kulmala, M., Worsnop, D. R., and Laaksonen, A.: An amorphous solid state of biogenic secondary organic aerosol particles. Nature, 467, 824-827, 2010.

Volkamer, R., Ziemann, P. J., and Molina, M. J.: Secondary Organic Aerosol Formation from Acetylene (C_2H_2): seed effect on SOA yields due to organic photochemistry in the aerosol aqueous phase. Atmos. Chem. Phys., 9, 1907–1928, 2009.

Wang, C., Lei, Y. D., Endo, S., and Wania, F.: Measuring and modeling the salting out effect in ammonium sulfate solutions. Environ. Sci. Technol., 48, 13238–13245, 2014.

Wania, F., Lei, Y. D., Wang, C., Abbatt, J. P. D., and Goss, K.-U.: Novel methods for predicting gas-particle partitioning during the formation of secondary organic aerosol. Atmos. Chem. Phys. 14, 13189-13204, 2014.

881 Wexler, A. S., and Clegg, S. L.: Atmospheric aerosol models for systems including the ions H^+,
882 NH_4^+, Na^+, SO_4^{2-}, NO_3^-, Cl^-, Br^- and H_2O. J. Geophys. Res. 107, No. D14, art. no. 4207,
883 doi:10.1029/2001JD000451, 2002.

884 Wong, F. and Wania, F.: Visualising the equilibrium distribution and mobility of organic
885 contaminants in soil using the chemical partitioning space. J. Environ. Monit., 13, 1569-1578,
886 2011.

887 Westgate, J. N. and Wania F.: Model-based exploration of the drivers of mountain cold-trapping
888 in soils. Environ. Sci.: Processes Impacts, 15, 2220-2232, 2013.

889 Wyche, K. P., Monks, P. S., Ellis, A. M., Cordell, R. L., Parker, A. E., Whyte, C., Metzger, A.,
890 Dommen, J., Duplissy, J., Prevot, A. S. H., Baltensperger, U., Rickard, A. R., and Wulfert, F.:
891 Gas phase precursors to anthropogenic secondary organic aerosol: detailed observations of 1,3,5-
892 trimethylbenzene photooxidation. Atmos. Chem. Phys., 9, 635-665, doi:10.5194/acp-9-635-
893 2009, 2009.

894 You, Y., Renbaum-Wolff, L., Carreras-Sospedra, M., Hanna, S. J., Hiranuma, N., Kamal, S.,
895 Smith, M. L., Zhang, X., Weber, R. J., Shilling, J. E., Dabdub, D., Martin, S. T., and Bertram,
896 A.: K. Images reveal that atmospheric particles can undergo liquid-liquid phase separations.
897 Proc. Nat. Acad. Sci. US, 109, 13188-13193, 2012.

898 Zuend, A. and Seinfeld, J. H.: Modeling the gas-particle partitioning of secondary organic
899 aerosol: the importance of liquid-liquid phase separation. Atmos. Chem. Phys., 12, 3857-3882,
900 2012.

Figure Captions

Figure 1 Different versions of the chemical partitioning space for the atmosphere, showing in red, blue and green the combinations of partitioning properties that lead to dominant equilibrium partitioning to the gas, aqueous, and water insoluble organic matter (WIOM) phase, respectively. Panel A refers to typical atmospheric conditions of 10 μg of both WIOM and liquid water per m^3 of air and demonstrates that the transition from 1 (10) % to 99 (90) % in a particular phase occurs over a four (two) order of magnitude range in a partition coefficient. A clear atmosphere (panel A and B), a cloud (C), and a dry chamber experiment (D) only differ in terms of the relative volume of the three phases present, leading to shifts in the thresholds indicating 50 % partitioning into any one phase. Dashed lines in panels B to D indicate the 50 % threshold for various loadings of WIOM and various liquid water contents.

Figure 2 Placement of the selected oxidation products of *n*-alkanes, biogenic terpenes and mono-aromatic hydrocarbons in the partitioning space. $K_{WIOM/G}$ and $K_{W/G}$ at 15 °C and 0 M salt of the compounds was estimated using SPARC assuming the solvation properties of WIOM can be approximated by those of structure B.

Figure 3 Same as Fig. 2, except that markers are coloured based on a chemical's number of carbon atoms (n_C) (left) or its average carbon oxidation state (OS_C).

Figure 4 Same as Fig. 2, except that different regions of the chemical partitioning space have been named according to the type of compounds that fall into these regions.

Figure 5 Arrows indicating the uncertainty of chemical placement in the partitioning space based on the discrepancy of $K_{WIOM/G}$ and $K_{W/G}$ predictions made with SPARC (origin of arrows), ppLFERs (tip of blue arrows) and COSMOtherm (tip of red arrows). For some compounds, no COSMOtherm predictions are available.

Figure 6 Placement of α-pinene and some of its oxidation products in the chemical partitioning space based on predictions with SPARC (left) and COSMOtherm (right). Each chemical is represented by three lines, which account for the

influence of temperature variations between 0 and 30 °C (diagonal line), the salting-out effect by 6.6 M $(NH_4)_2SO_4$ (vertical line) and the polarity of the surrogate representing the solvation properties of WIOM (horizontal line). The chemicals are superimposed on the dominant phase distribution maps for wet aerosol (left) and a cloud (right). The red lines encircle regions where chemicals fall whose contribution to SOA formation would not be considered, if the aqueous phase in an aerosol (solid line) or in a cloud (dashed line) were ignored.

Figure 7 Oxidation products of the *n*-alkane with 17 carbon atoms placed within the chemical partitioning space based on partition coefficients at 25 °C predicted with ppLFERs and connected by arrows based on sequence of reaction by which they are formed. The code names for the compounds are based on Jordan et al. (2008).

Figure 8 Displacement of chemicals in the partitioning space caused by transformations involved in the oxidation of *n*-alkanes with 10 (blue) and 17 (green) carbons using predictions of $K_{WIOM/G}$ and $K_{W/G}$ at 25 °C obtained by ppLFER. Also given are the mean vertical displacement (MVD) and mean horizontal displacement (MHD).

Figure 9 Displacement in the chemical partitioning space occurring upon the addition of a hydroxyl (A) or nitro-group (B) to a mono-aromatic hydrocarbon, as predicted by SPARC for 15 °C and using structure B for WIOM (VD: vertical displacement, HD: horizontal displacement).

Figure 10 Displacements in the chemical partitioning space due to various dimerisation reactions proposed for ozonolysis reaction products of α-pinene by Camredon et al. (2010). $K_{WIOM/G}$ and $K_{W/G}$ at 15 °C were estimates with SPARC using structure B as a surrogate for WIOM. Also shown is the categorisation into compounds with different atmospheric phase distribution behaviour introduced in Fig. 4.

Figure 11 Visualisation in the partitioning space of processes occurring during the oxidation of VOC precursors in a chamber experiment or a photochemical smog episode (in the presence of water). While the addition of functional groups and dimerisation reactions lead to an increase in $K_{WIOM/G}$ and $K_{W/G}$ and therefore a gradual shift to the lower right, the attendant increase in the organic aerosol load shifts the threshold for the gas-WIOM transition to the left.

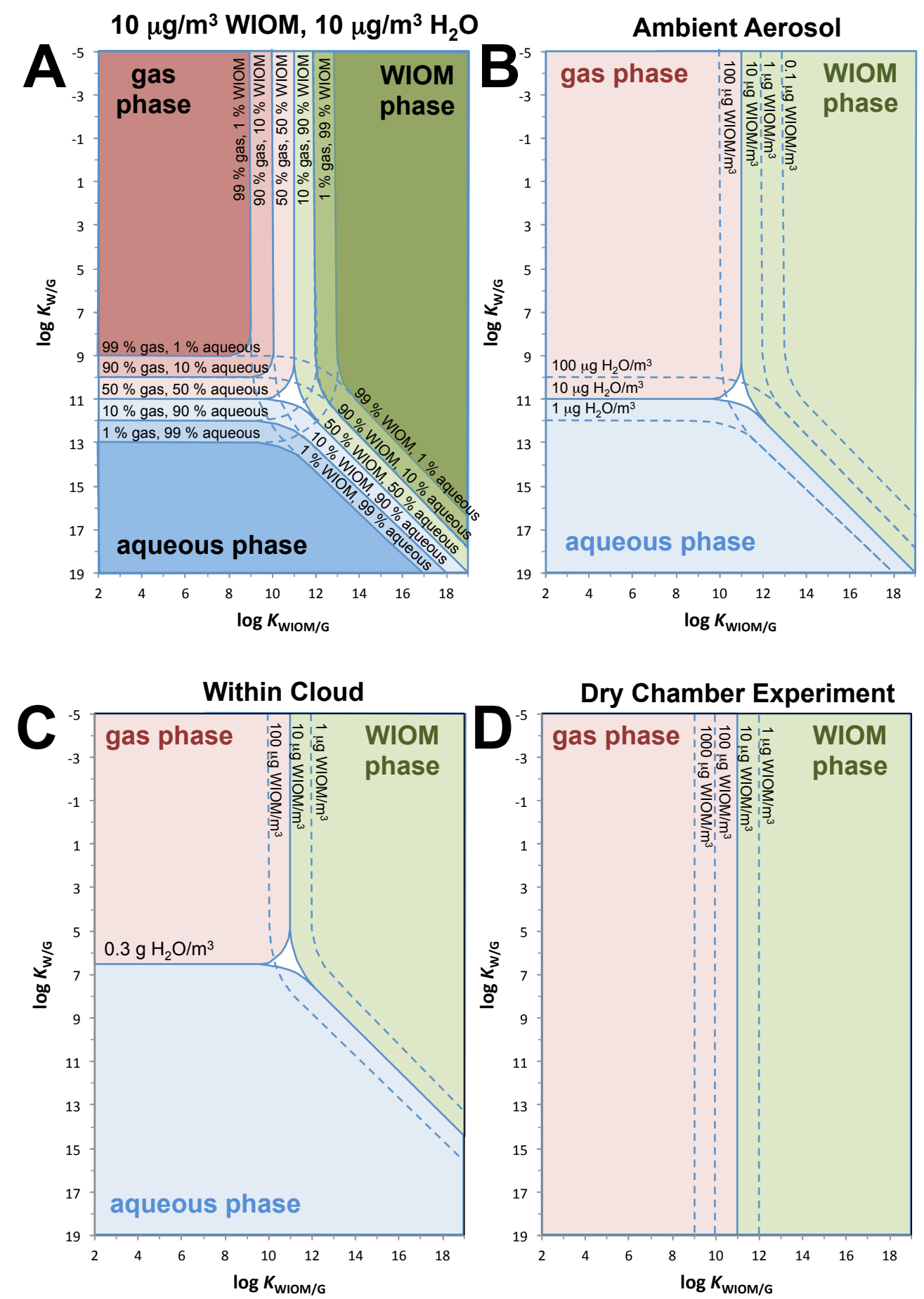
A
10 μg/m³ WIOM, 10 μg/m³ H2O
gas phase
WIOM phase
aqueous phase
99 % gas, 1 % WIOM
90 % gas, 10 % WIOM
50 % gas, 50 % WIOM
10 % gas, 90 % WIOM
1 % gas, 99 % WIOM
99 % gas, 1 % aqueous
90 % gas, 10 % aqueous
50 % gas, 50 % aqueous
10 % gas, 90 % aqueous
1 % gas, 99 % aqueous
99 % WIOM, 1 % aqueous
90 % WIOM, 10 % aqueous
50 % WIOM, 50 % aqueous
10 % WIOM, 90 % aqueous
1 % WIOM, 99 % aqueous
log KW/G
log KWIOM/G
B
Ambient Aerosol
gas phase
WIOM phase
aqueous phase
100 μg WIOM/m³
10 μg WIOM/m³
1 μg WIOM/m³
0.1 μg WIOM/m³
100 μg H2O/m³
10 μg H2O/m³
1 μg H2O/m³
log KW/G
log KWIOM/G
C
Within Cloud
gas phase
WIOM phase
aqueous phase
100 μg WIOM/m³
10 μg WIOM/m³
1 μg WIOM/m³
0.3 g H2O/m³
log KW/G
log KWIOM/G
D
Dry Chamber Experiment
gas phase
WIOM phase
1000 μg WIOM/m³
100 μg WIOM/m³
10 μg WIOM/m³
1 μg WIOM/m³
log KW/G
log KWIOM/G

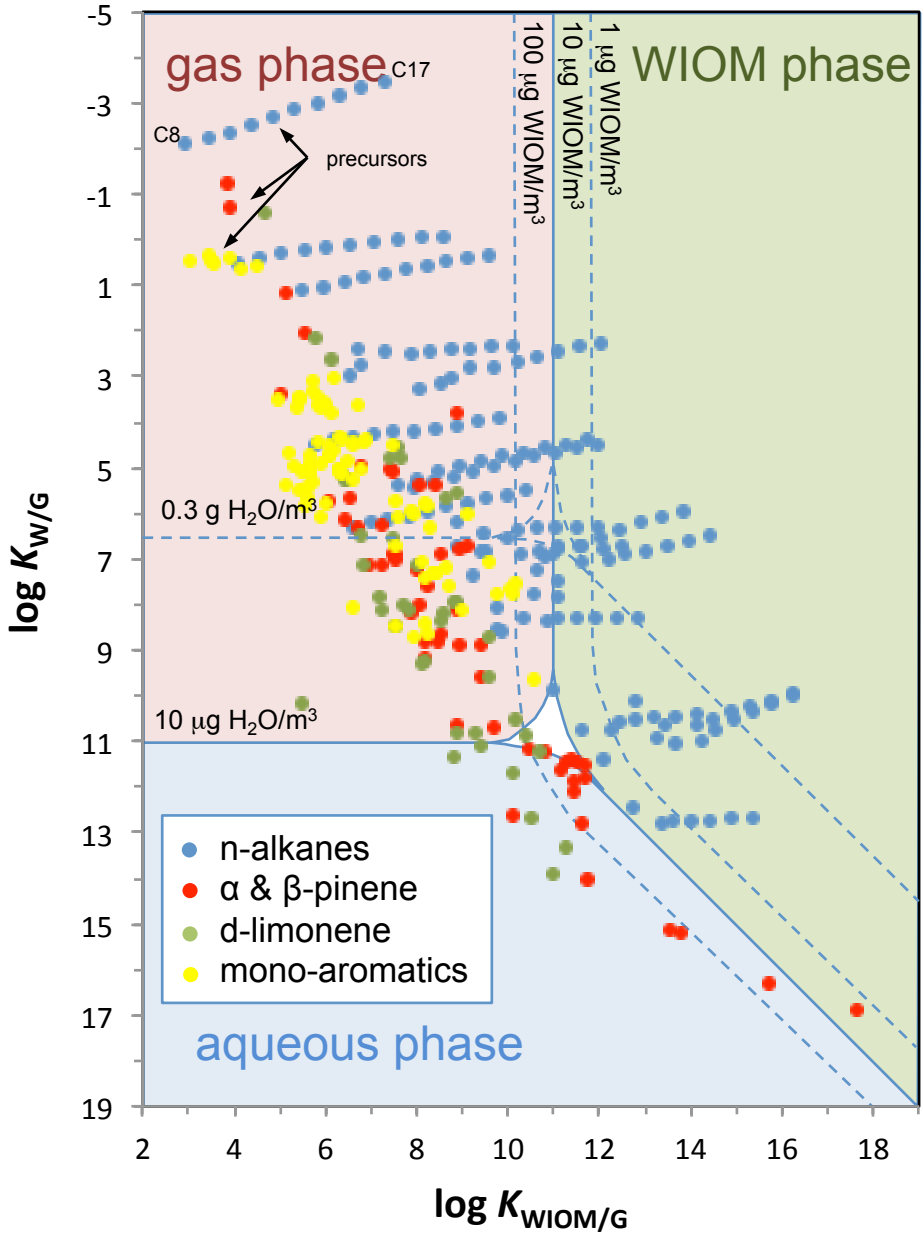
gas phase
C17
C8
precursors
100 μg WIOM/m³
10 μg WIOM/m³
1 μg WIOM/m³
WIOM phase
0.3 g H2O/m³
10 μg H2O/m³
n-alkanes
α & β-pinene
d-limonene
mono-aromatics
aqueous phase
log KW/G
log KWIOM/G
-5
-3
-1
1
3
5
7
9
11
13
15
17
19
2
4
6
8
10
12
14
16
18

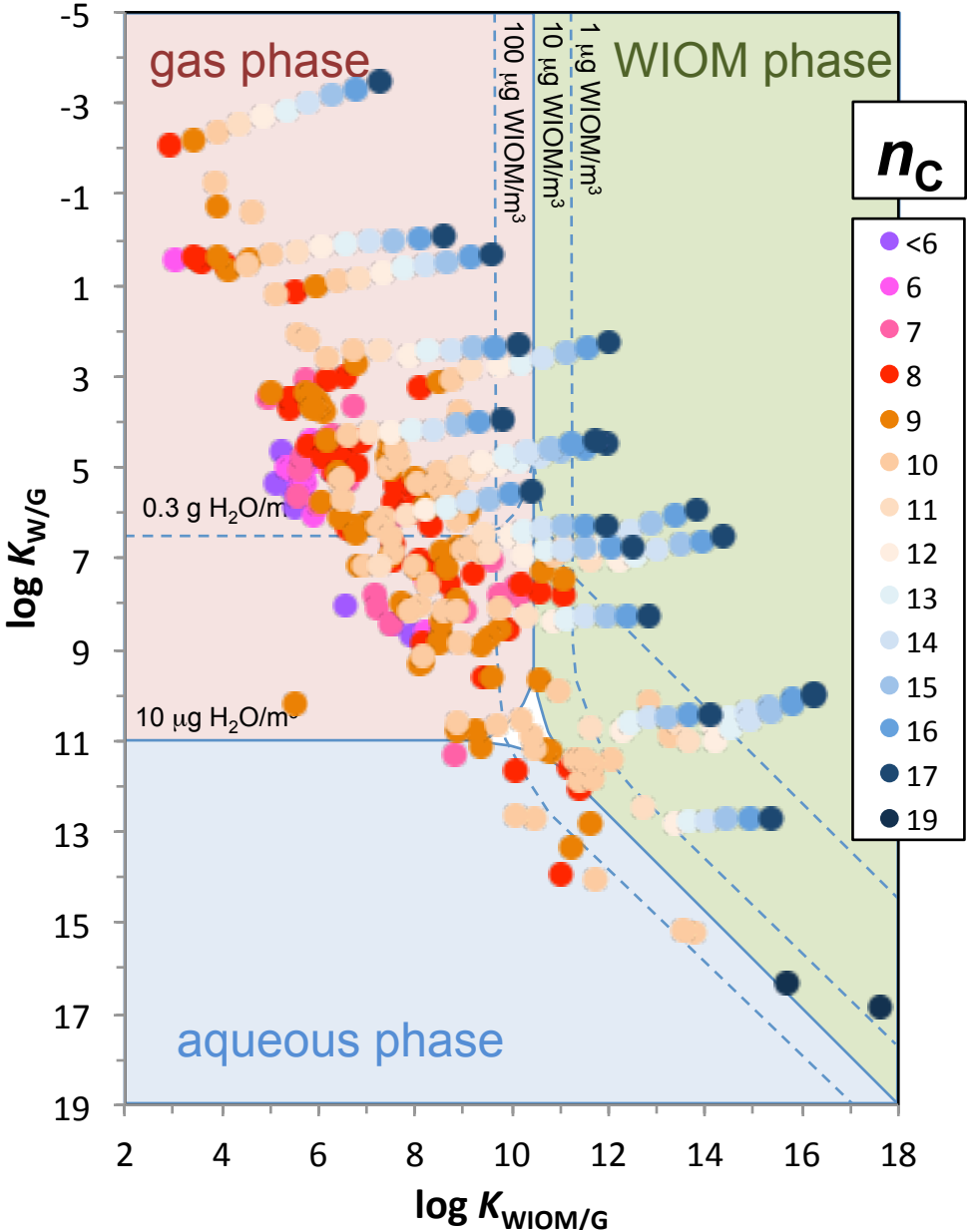
gas phase
WIOM phase
aqueous phase
100 µg WIOM/m³
10 µg WIOM/m³
1 µg WIOM/m³
0.3 g H2O/m
10 µg H2O/m
nC
<6
6
7
8
9
10
11
12
13
14
15
16
17
19
log KW/G
log KWIOM/G
-5
-3
-1
1
3
5
7
9
11
13
15
17
19
2
4
6
8
10
12
14
16
18

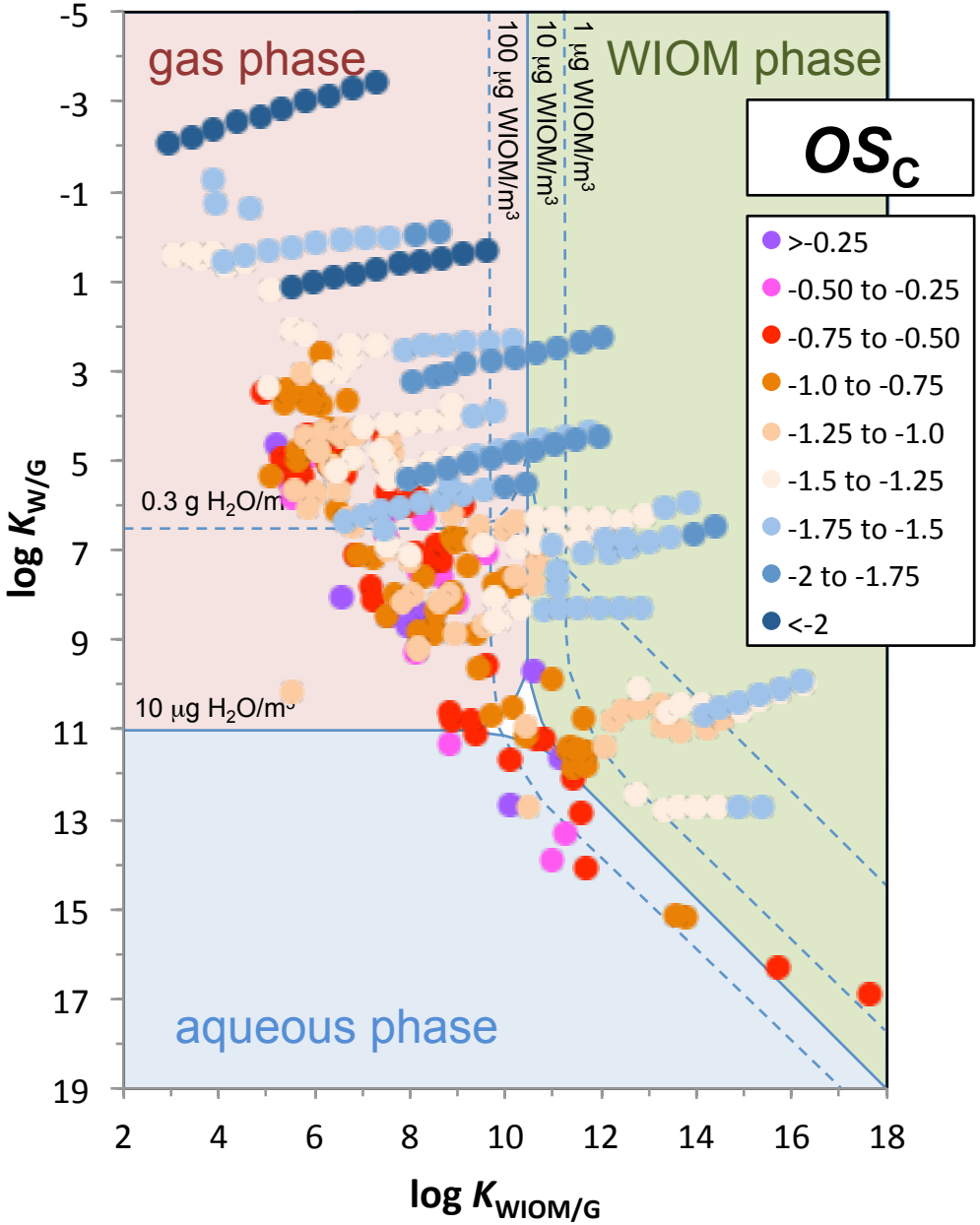
gas phase
WIOM phase
aqueous phase
100 µg WIOM/m³
10 µg WIOM/m³
1 µg WIOM/m³
0.3 g H2O/m³
10 µg H2O/m³
OSC
>-0.25
-0.50 to -0.25
-0.75 to -0.50
-1.0 to -0.75
-1.25 to -1.0
-1.5 to -1.25
-1.75 to -1.5
-2 to -1.75
<-2
log KW/G
log KWIOM/G
-5
-3
-1
1
3
5
7
9
11
13
15
17
19
2
4
6
8
10
12
14
16
18

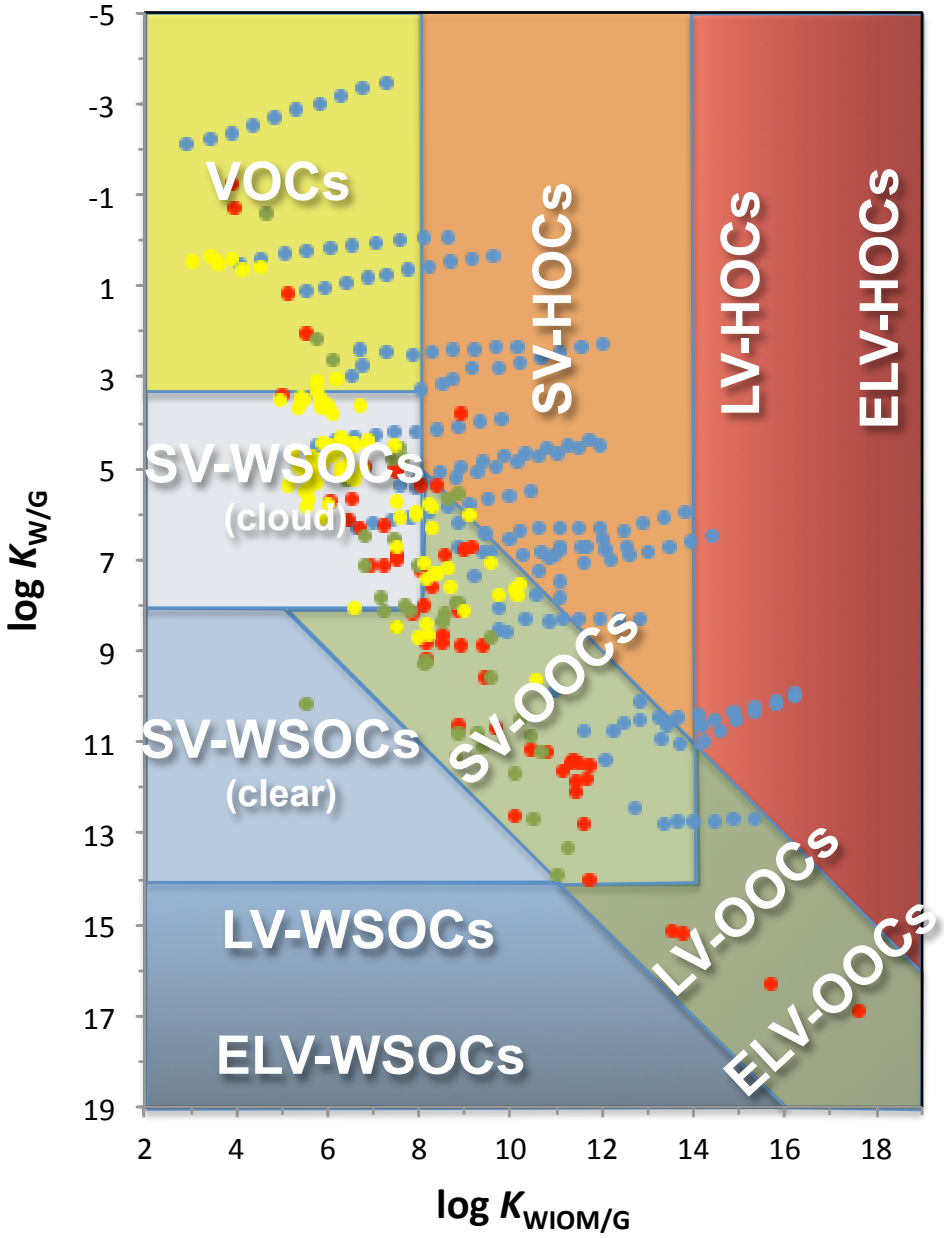
VOCs
SV-HOCs
LV-HOCs
ELV-HOCs
SV-WSOCs
(cloud)
SV-OOCs
SV-WSOCs
(clear)
LV-WSOCs
LV-OOCs
ELV-OOCs
ELV-WSOCs
-5
-3
-1
1
3
5
7
9
11
13
15
17
19
2
4
6
8
10
12
14
16
18
log $K_{W/G}$
log $K_{WIOM/G}$

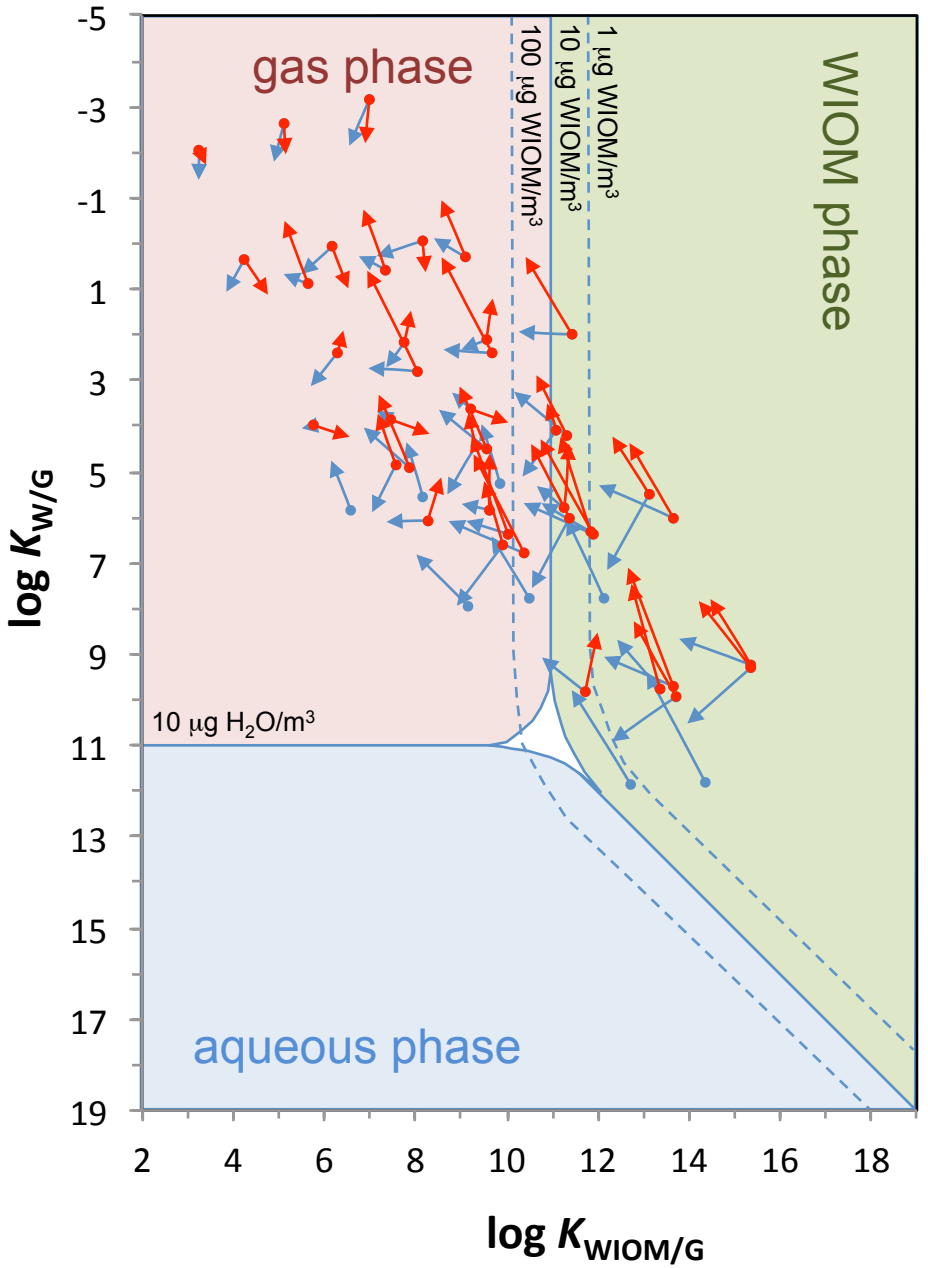

n-alkanes

(C9, C13, C17)

25 °C
0 M salt
WIOM B

Origin of arrow:
SPARC-prediction

ppLFER
COSMOtherm

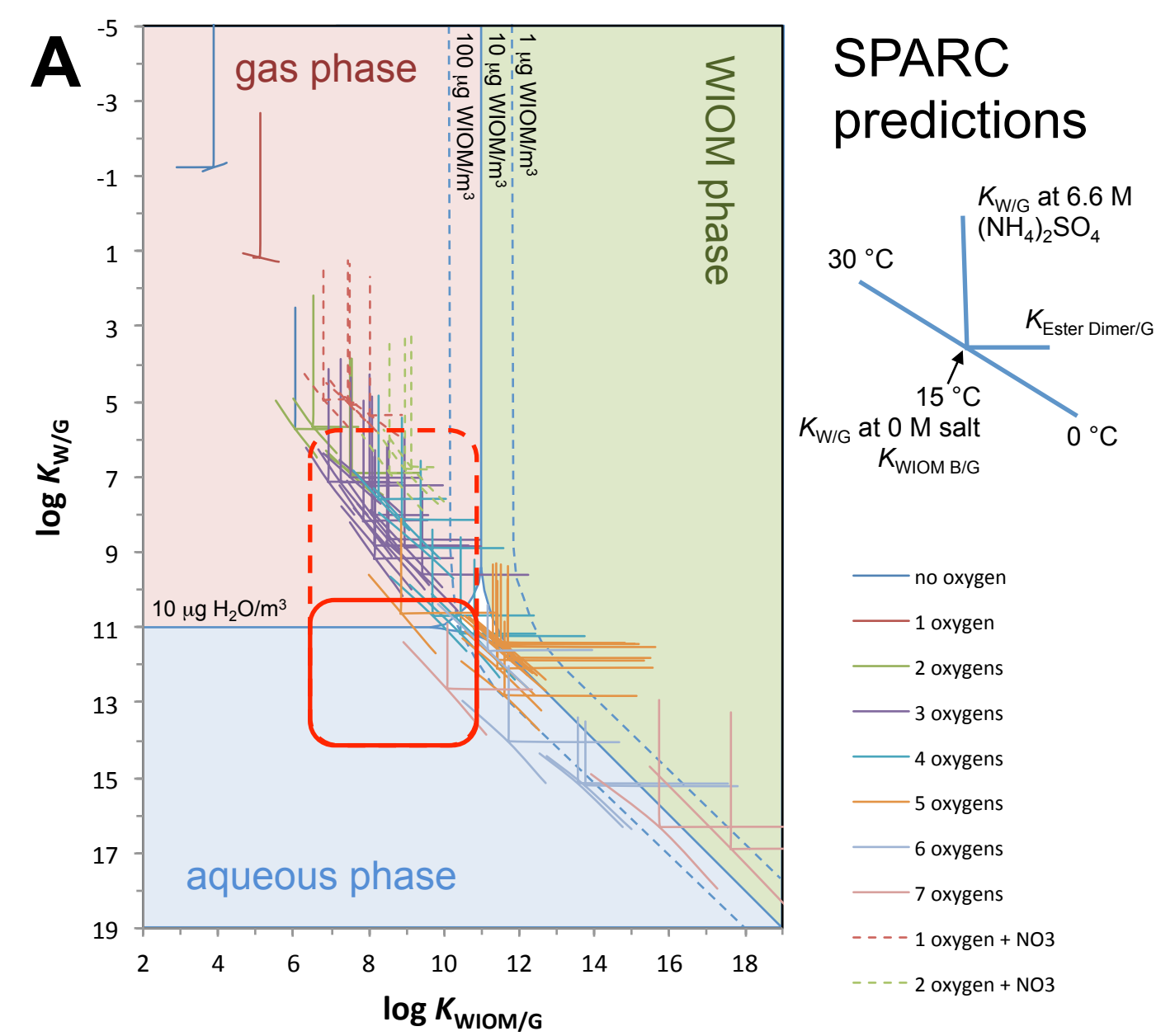
A
gas phase
aqueous phase
WIOM phase
100 μg WIOM/m³
10 μg WIOM/m³
1 μg WIOM/m³
10 μg H2O/m³
log KW/G
log KWIOM/G
-5
-3
-1
1
3
5
7
9
11
13
15
17
19
2
4
6
8
10
12
14
16
18
SPARC predictions
KW/G at 6.6 M (NH4)2SO4
30 °C
KEster Dimer/G
15 °C
KW/G at 0 M salt
KWIOM B/G
0 °C
no oxygen
1 oxygen
2 oxygens
3 oxygens
4 oxygens
5 oxygens
6 oxygens
7 oxygens
1 oxygen + NO3
2 oxygen + NO3

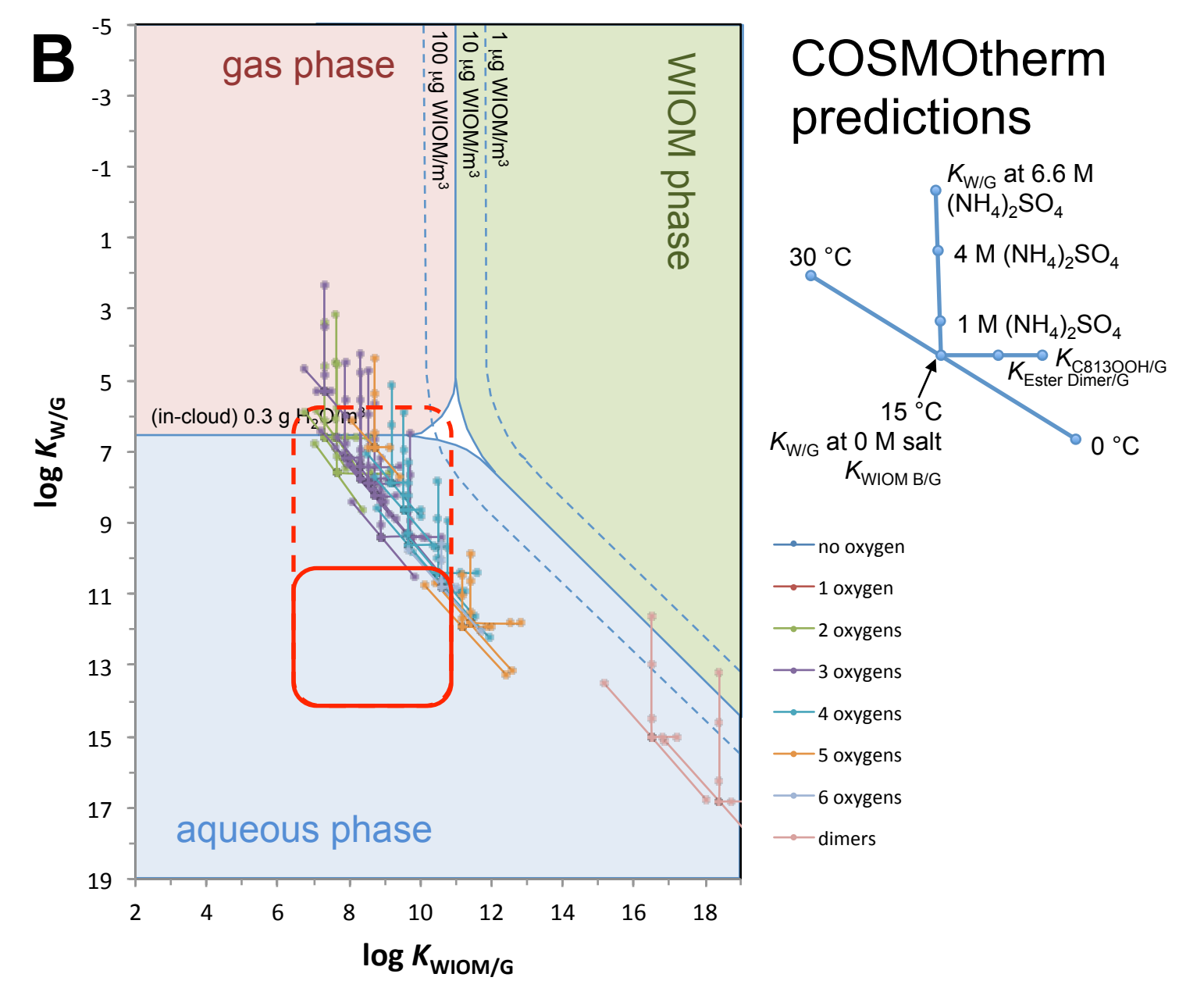
B
gas phase
100 µg WIOM/m³
10 µg WIOM/m³
1 µg WIOM/m³
WIOM phase
(in-cloud) 0.3 g H2O/m³
aqueous phase
log KW/G
log KWIOM/G
-5
-3
-1
1
3
5
7
9
11
13
15
17
19
2
4
6
8
10
12
14
16
18
COSMOtherm predictions
KW/G at 6.6 M (NH4)2SO4
4 M (NH4)2SO4
30 °C
1 M (NH4)2SO4
KC813OOH/G
KEster Dimer/G
15 °C
0 °C
KW/G at 0 M salt
KWIOM B/G
no oxygen
1 oxygen
2 oxygens
3 oxygens
4 oxygens
5 oxygens
6 oxygens
dimers

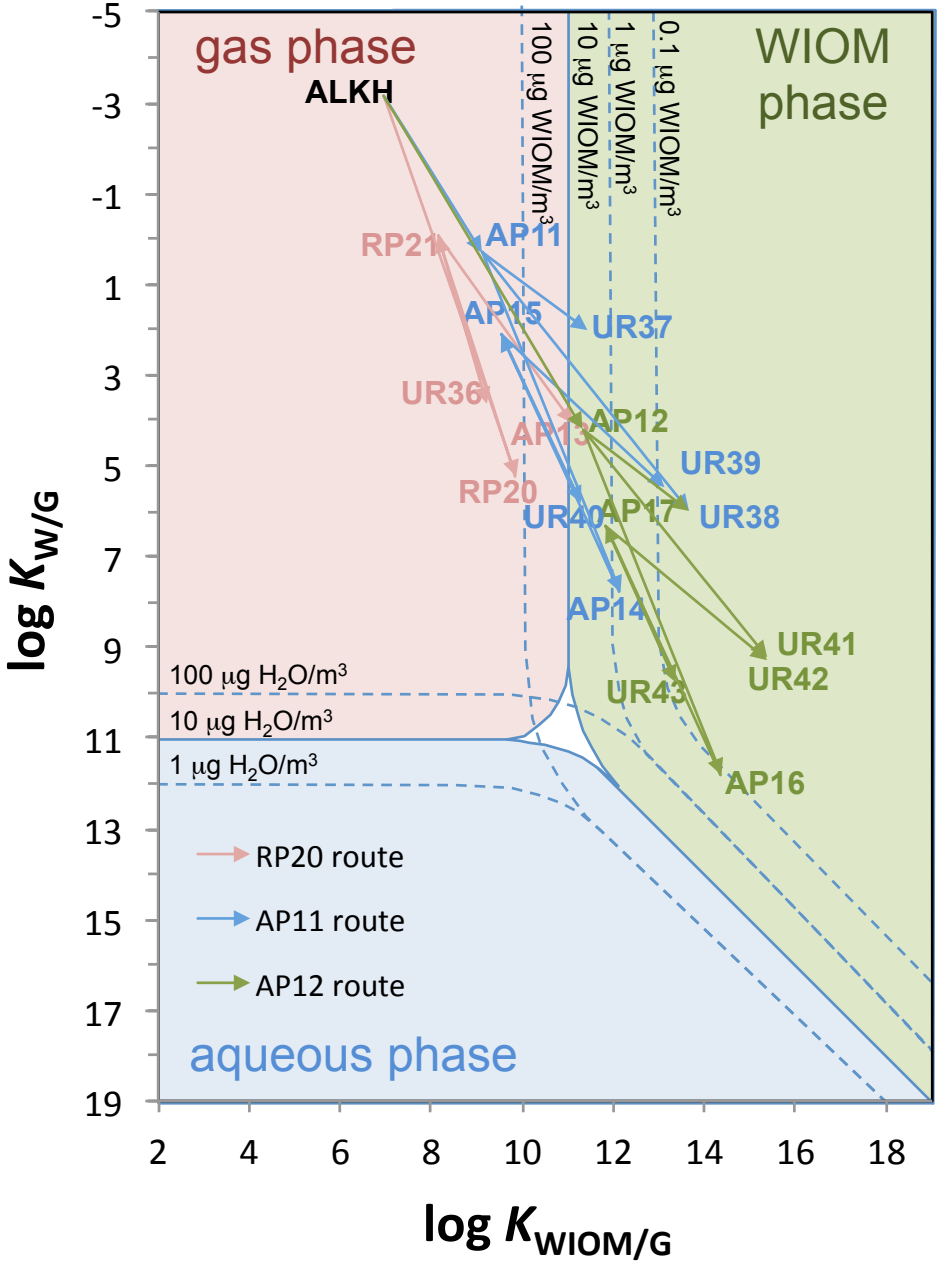
gas phase
WIOM phase
aqueous phase
ALKH
RP21
AP11
AP15
UR37
UR36
AP13
AP12
UR39
RP20
UR40
AP17
UR38
AP14
UR41
UR42
UR43
AP16
100 µg WIOM/m³
10 µg WIOM/m³
1 µg WIOM/m³
0.1 µg WIOM/m³
100 µg H2O/m³
10 µg H2O/m³
1 µg H2O/m³
RP20 route
AP11 route
AP12 route
log K_W/G
log K_WIOM/G
-5
-3
-1
1
3
5
7
9
11
13
15
17
19
2
4
6
8
10
12
14
16
18

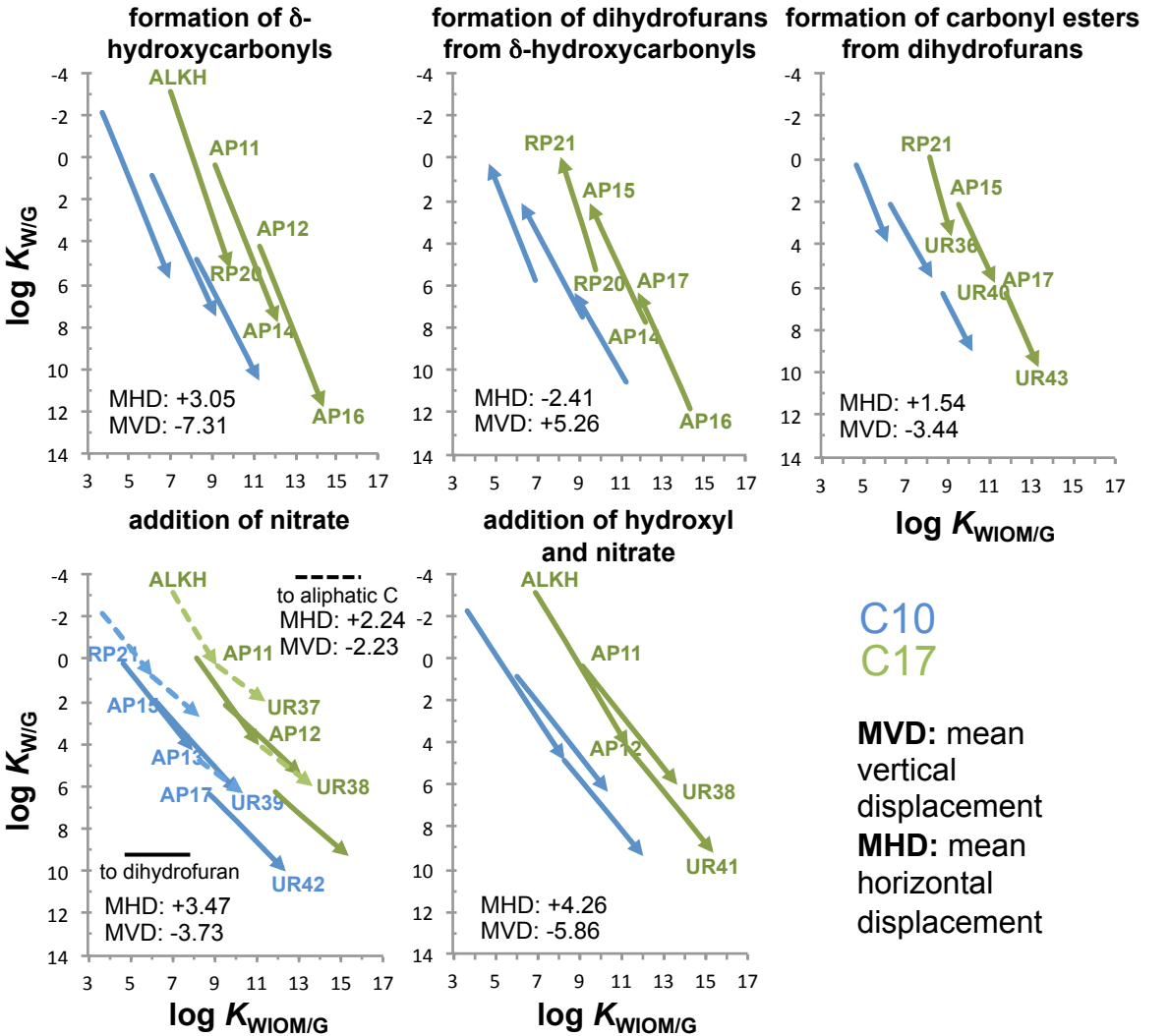
formation of δ-hydroxycarbonyls
ALKH
AP11
AP12
RP20
AP14
AP16
MHD: +3.05
MVD: -7.31
formation of dihydrofurans from δ-hydroxycarbonyls
RP21
AP15
RP20
AP17
AP14
AP16
MHD: -2.41
MVD: +5.26
formation of carbonyl esters from dihydrofurans
RP21
AP15
UR36
UR40
AP17
UR43
MHD: +1.54
MVD: -3.44
addition of nitrate
ALKH
to aliphatic C
MHD: +2.24
MVD: -2.23
RP21
AP11
AP15
UR37
AP12
AP13
UR38
AP17
UR39
UR42
to dihydrofuran
MHD: +3.47
MVD: -3.73
addition of hydroxyl and nitrate
ALKH
AP11
AP12
UR38
UR41
MHD: +4.26
MVD: -5.86
log $K_{W/G}$
log $K_{WIOM/G}$
C10
C17
MVD: mean vertical displacement
MHD: mean horizontal displacement

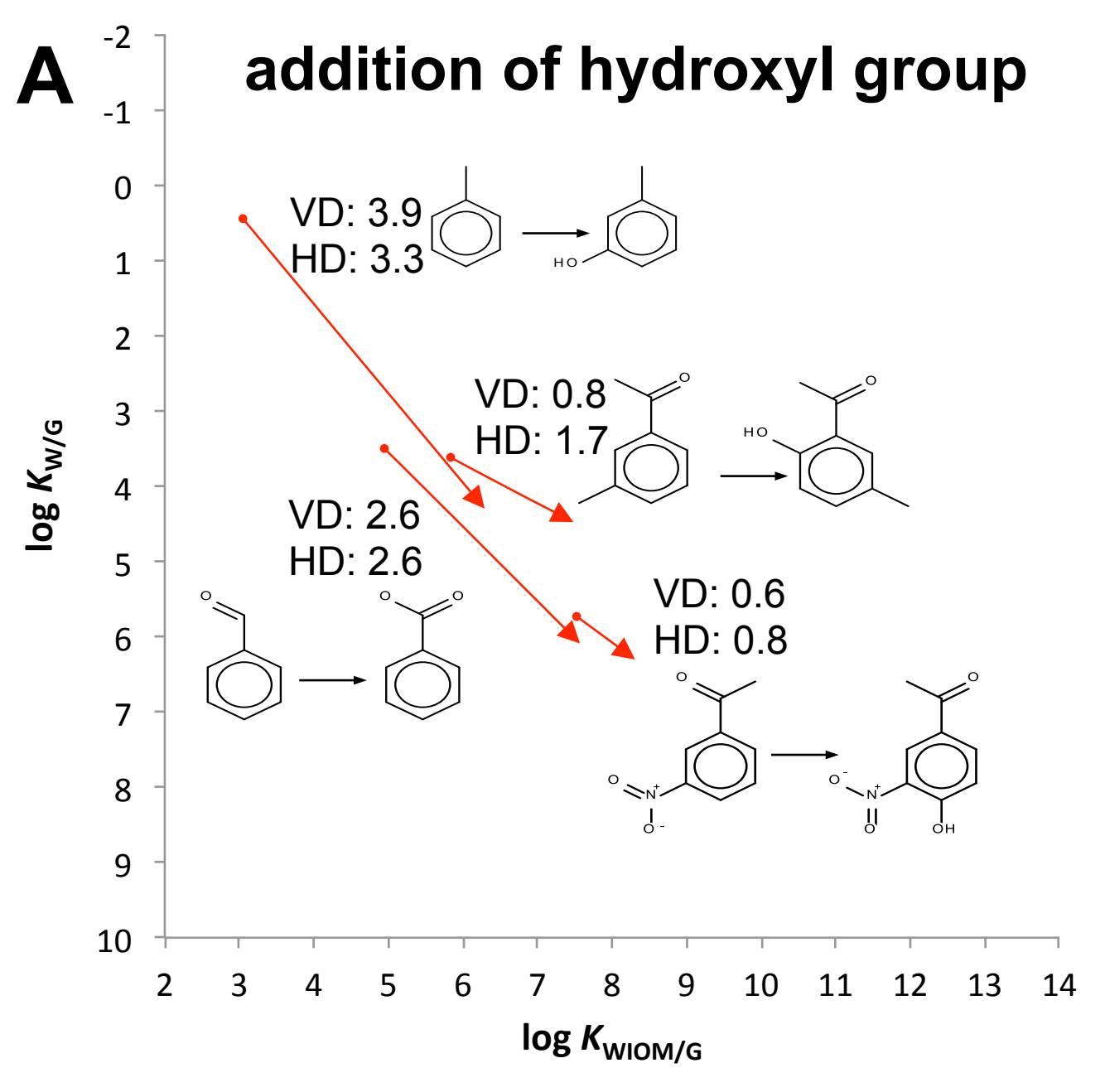
A
addition of hydroxyl group
VD: 3.9
HD: 3.3
VD: 0.8
HD: 1.7
VD: 2.6
HD: 2.6
VD: 0.6
HD: 0.8
HO
HO
OH
log $K_{W/G}$
log $K_{WIOM/G}$
-2
-1
0
1
2
3
4
5
6
7
8
9
10
2
3
4
5
6
7
8
9
10
11
12
13
14

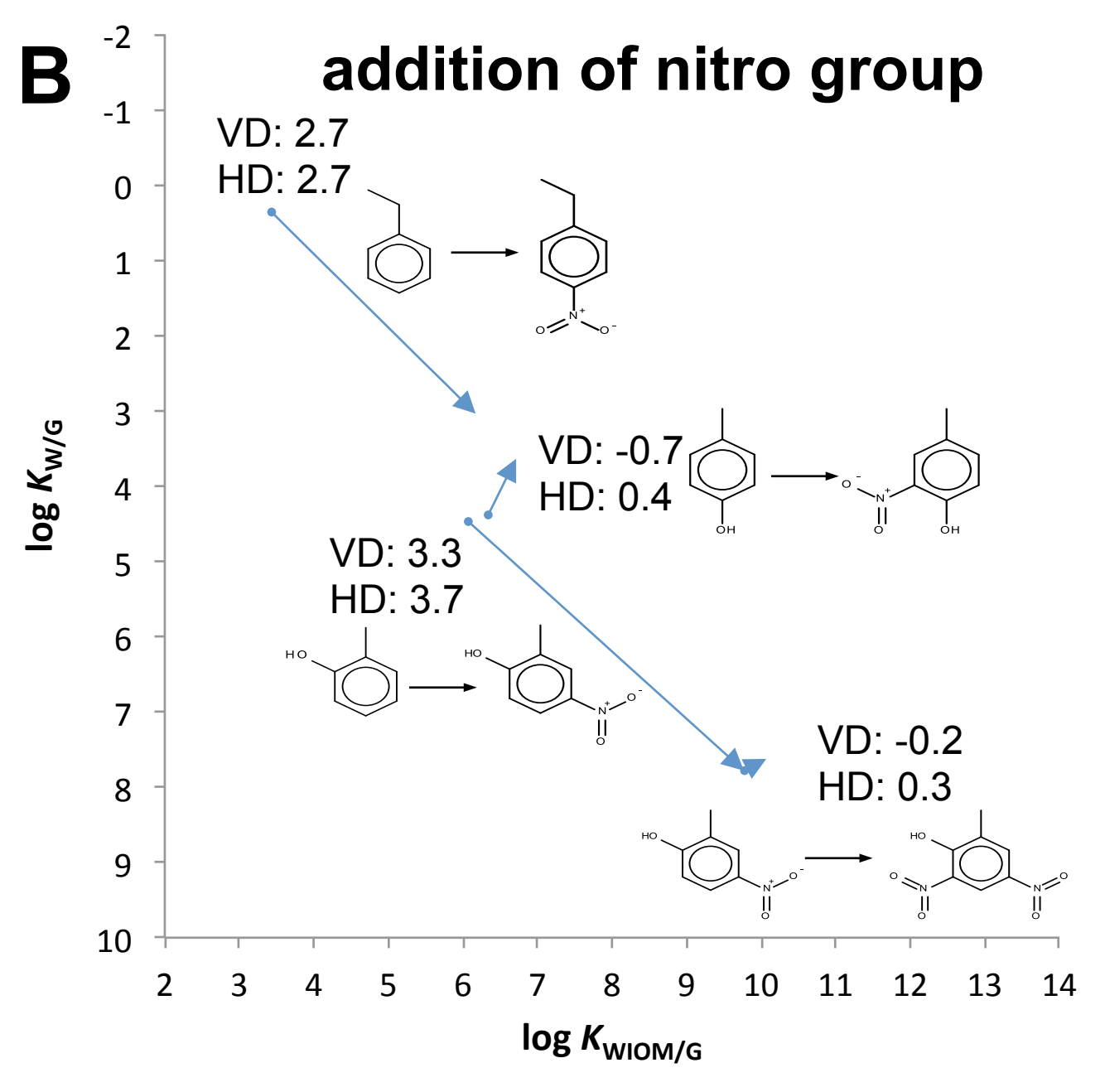
B
addition of nitro group
VD: 2.7
HD: 2.7
VD: -0.7
HD: 0.4
VD: 3.3
HD: 3.7
VD: -0.2
HD: 0.3
log $K_{W/G}$
log $K_{WIOM/G}$
-2
-1
0
1
2
3
4
5
6
7
8
9
10
2
3
4
5
6
7
8
9
10
11
12
13
14

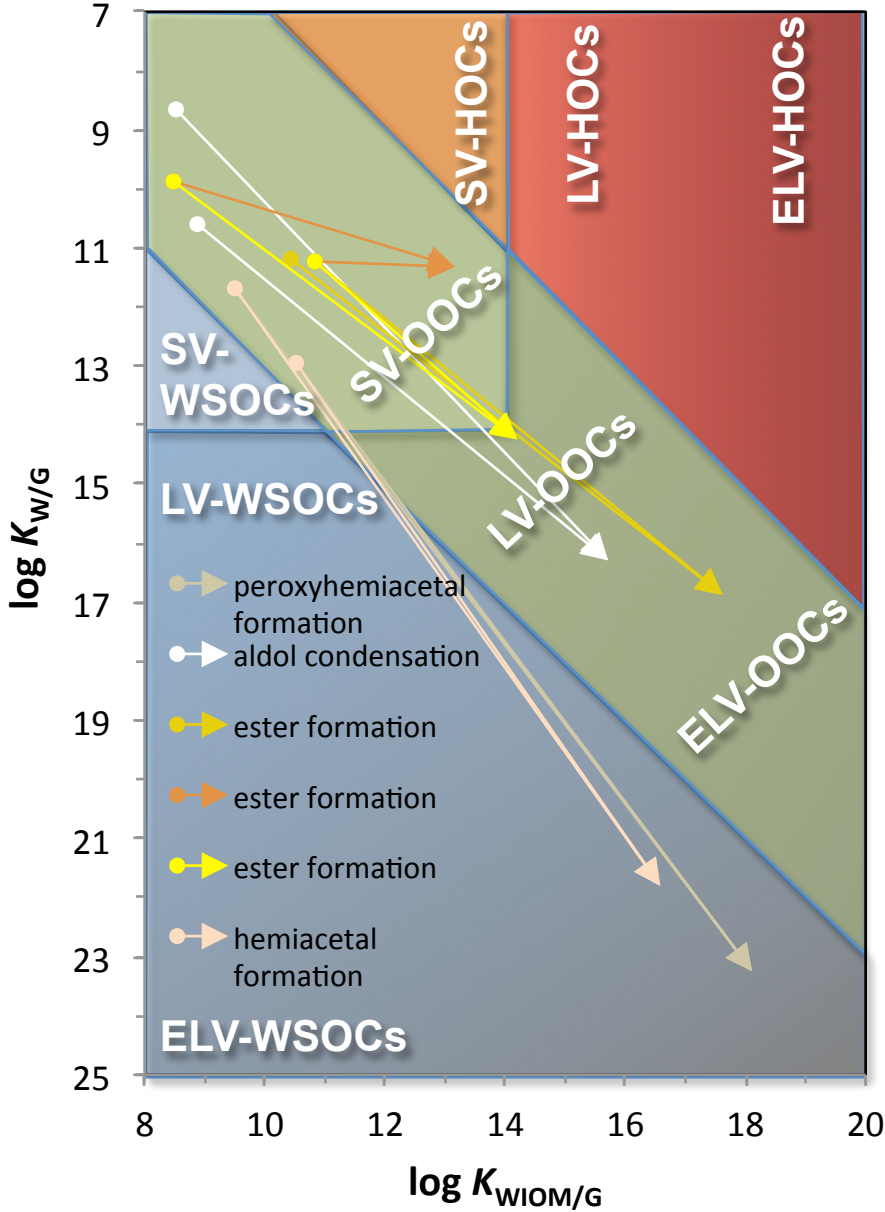
SV-HOCs
LV-HOCs
ELV-HOCs
SV-OOCs
LV-OOCs
ELV-OOCs
SV-WSOCs
LV-WSOCs
ELV-WSOCs
peroxyhemiacetal formation
aldol condensation
ester formation
ester formation
ester formation
hemiacetal formation
log $K_{W/G}$
log $K_{WIOM/G}$
7
9
11
13
15
17
19
21
23
25
8
10
12
14
16
18
20

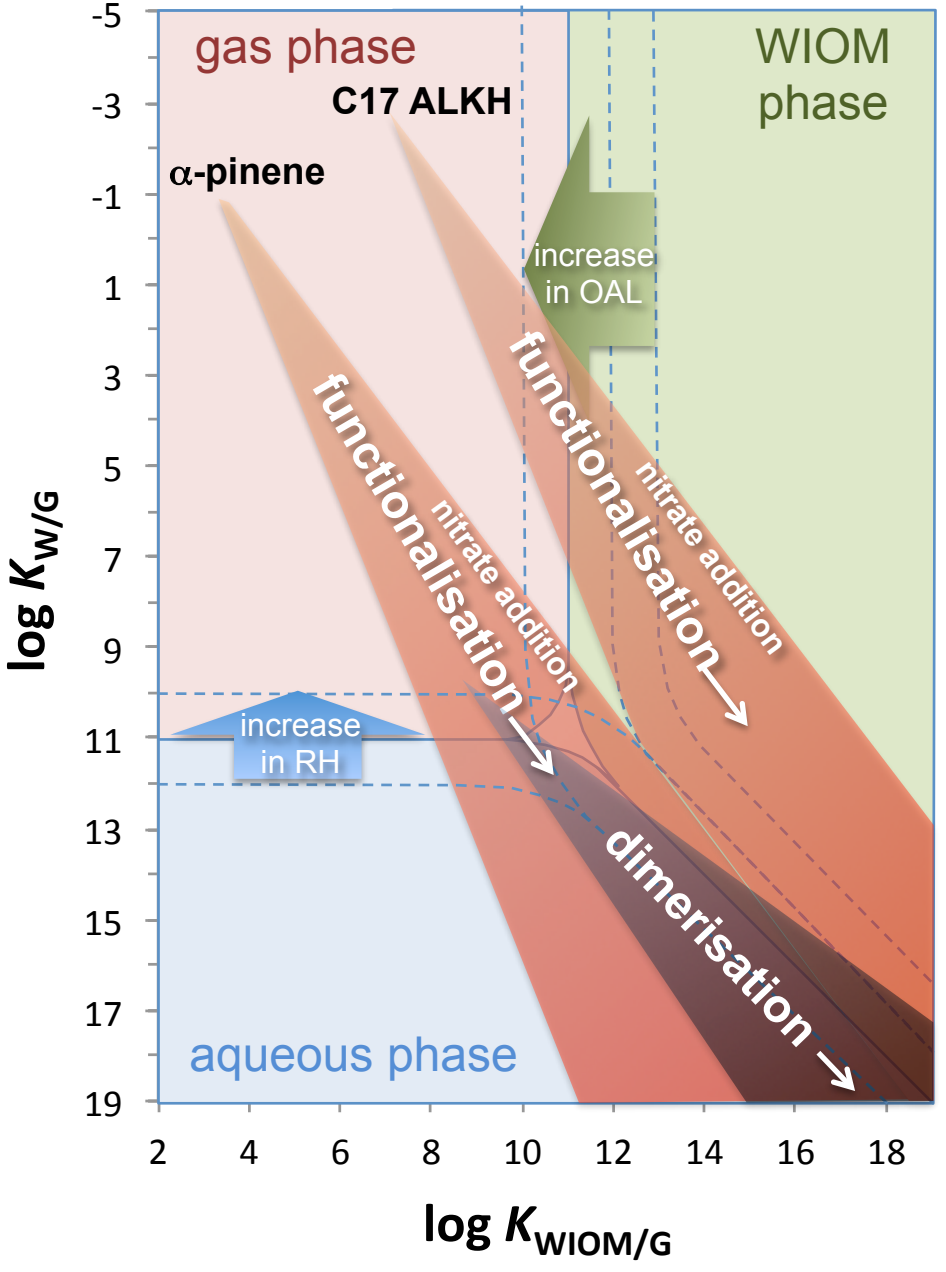
gas phase
C17 ALKH
α-pinene
WIOM phase
increase in OAL
functionalisation
nitrate addition
functionalisation
nitrate addition
increase in RH
dimerisation
aqueous phase
-5
-3
-1
1
3
5
7
9
11
13
15
17
19
2
4
6
8
10
12
14
16
18
log $K_{W/G}$
log $K_{WIOM/G}$